Inorg. Chem. **2005**, *44*, 4555–4567

New Polynuclear Manganese Clusters from the Use of the Hydrophobic Carboxylate Ligand 2,2-Dimethylbutyrate

Nicole E. Chakov,[†] Lev N. Zakharov,[‡] Arnold L. Rheingold,[‡] Khalil A. Abboud,[†] and George Christou*[,†]

Department of Chemistry, University of Florida, Gainesville, Florida 32611-7200, and Department of Chemistry—0358, University of California at San Diego, La Jolla, California 92093-0358

Received February 4, 2005

The syntheses, structures, and magnetic properties are reported of $[Mn_{12}O_{12}(O_2CPe^t)_{16}(MeOH)_4]$ (**4**), $[Mn_6O_2(O_2CH_2)(O_2CPe^t)_{11}(HO_2CPe^t)_2(O_2CMe)]$ (**5**), $[Mn_9O_6(OH)(CO_3)(O_2CPe^t)_{12}(H_2O)_2]$ (**6**), and $[Mn_4O_2(O_2CPe^t)_6(bpy)_2]$ (**7**, bpy = 2,2′-bipyridine), where Pe^t = *tert*-pentyl (Pe^tCO_2H = 2,2-dimethylbutyric acid). These complexes were all prepared from reactions of $[Mn_{12}O_{12}(O_2CPe^t)_{16}(H_2O)_4]$ (**3**) in CH_2Cl_2. Complex **4**·2MeCN crystallizes in the triclinic space group $P\bar{1}$ and contains a central $[Mn^{IV}_4O_4]$ cubane core that is surrounded by a nonplanar ring of eight alternating Mn^{III} and eight μ_3-O^{2-} ions. This is only the third Mn_{12} complex in which the four bound water molecules have been replaced by other ligands, in this case MeOH. Complex **5**·$^1/_2CH_2Cl_2$ crystallizes in the monoclinic space group $P2_1/c$ and contains two $[Mn_3(\mu_3\text{-}O)]^{7+}$ units linked at two of their apexes by two $Pe^tCO_2^-$ ligands and one μ_4-$CH_2O_2^{2-}$ bridge. The complex is a new structural type in Mn chemistry, and also contains only the third example of a gem-diolate unit bridging four metal ions. Complex **6**·H_2O·Pe^tCO_2H crystallizes in the orthorhombic space group $Cmc2_1$ and possesses a $[Mn^{III}_9(\mu_3\text{-}O)_6(\mu\text{-}OH)(\mu_3\text{-}CO_3)]^{12+}$ core. The molecule contains a μ_3-CO_3^{2-} ion, the first example in a discrete Mn complex. Complex **7**·$2H_2O$ crystallizes in the monoclinic space group $P2_1/c$ and contains a known $[Mn^{III}_2Mn^{II}_2(\mu_3\text{-}O)_2]^{6+}$ core that can be considered as two edge-sharing, triangular $[Mn_3O]$ units. Additionally, the synthesis and magnetic properties of a new enneanuclear cluster of formula $[Mn_9O_7(O_2CCH_2Bu^t)_{13}(THF)_2]$ (**8**, THF = tetrahydrofuran) are reported. The molecule was obtained by the reaction of $[Mn_{12}O_{12}(O_2CCH_2Bu^t)_{16}(H_2O)_4]$ (**2**) with THF. Complexes **2** and **4** display quasireversible redox couples when examined by cyclic voltammetry in CH_2Cl_2; oxidations are observed at –0.07 V (**2**) and –0.21 V (**4**) vs ferrocene. The magnetic properties of complexes **4**–**8** have been studied by direct current (DC) and alternating current (AC) magnetic susceptibility techniques. The ground-state spin of **4** was established by magnetization measurements in the 1.80–4.00 K and 0.5–7 T ranges. Fitting of the reduced magnetization data by full matrix diagonalization, incorporating a full powder average and including only axial anisotropy, gave $S = 10$, $g = 2.0(1)$, and $D = -0.39(10)$ cm^{-1}. The complex exhibits two frequency-dependent out-of-phase AC susceptibility signals (χ_M'') indicative of slow magnetization relaxation. An Arrhenius plot obtained from χ_M'' vs T data gave an effective energy barrier to relaxation (U_{eff}) of 62 and 35 K for the slower and faster relaxing species, respectively. These studies suggest that complex **4** is a single-molecule magnet (SMM). DC susceptibility studies on complexes **5**–**8** display overall antiferromagnetic behavior and indicate ground-state spin values of $S \leq 2$. AC susceptibility studies at <10 K confirm these small values and indicate the population of low-lying excited states even at these low temperatures. This supports the small ground-state spin values to be due to spin frustration effects.

Introduction

One of the principal motivations for the continuing exploration of manganese carboxylate chemistry is the established potential of this area as a rich source of single-molecule magnets (SMMs),[1–3] a field that began in 1993 when it was shown that $[Mn_{12}O_{12}(O_2CMe)_{16}(H_2O)_4]$·$2MeCO_2H$·$4H_2O$ (**1**) functions as a magnet at temperatures below its blocking temperature, T_B. A SMM possesses a significant potential energy barrier (U) to relaxation of its

* E-mail: christou@chem.ufl.edu.
† University of Florida.
‡ University of California at San Diego.

10.1021/ic050201+ CCC: $30.25
Published on Web 05/27/2005

magnetization vector, arising from the combination of a large-spin ground state, S, and a large, negative magnetoanisotropy of the easy-axis (or Ising) type (negative axial zero-field splitting parameter, D). The upper limit of this energy barrier is given by $S^2|D|$ and $(S^2 - {}^1/_4)|D|$ for integer and half-integer S values, respectively.[1,2] Experimental evidence for the slow, superparamagnet-like magnetic relaxation of a SMM is provided by the observation of hysteresis, the classical macroscale property of a magnet, in magnetization versus direct current (DC) field scans, and also by the observation of frequency-dependent, out-of-phase alternating current (AC) susceptibility signals (χ_M'').[4]

The calculated energy barrier, U, of complex **1** is 50 cm^{-1} (72 K), arising from $S = 10$ and $D = -0.50$ cm^{-1} (-0.72 K).[2a] This energy barrier allows molecules of complex **1** to function as individual magnets at low temperatures. The half-life for magnetization decay is so long that it is hardly measurable if molecules of **1** are magnetized at 1.5 K by applying a magnetic field and then removing the field.[2a] After more than a decade of research in this area, complex **1** and carboxylate-substituted derivatives still remain the molecules that function as magnets at the highest temperatures, exhibiting the most promise for use in high-density memory storage devices or in quantum computing. This is despite the preparation of many SMMs of a different structural type, as well as research in other areas such as molecular magnetism.

There are two main routes to new SMMs. The first is the modification of a given structural type in some way that does not change the core structure. For example, such studies on Mn_{12} complexes have included variation of the peripheral carboxylate ligation,[5,6] variation of the oxidation level by cluster reduction,[5a,7] replacement of some of the Mn centers with either Fe or Cr,[8,9] and replacement of some of the carboxylate ligands with non-carboxylate groups.[10−13] The second is the use of harsher conditions, such as the reaction of a cluster with a chelating ligand, that will often cause a core structural and/or nuclearity change leading to new structural types.[14] These methods have together afforded many new Mn_x species when a Mn_{12} complex was employed, such as $[Mn_{12}O_{12}(O_2CCH_2Bu^t)_{16}(H_2O)_4]$,[15] $[Mn_{30}O_{24}(OH)_8(O_2CCH_2Bu^t)_{32}(H_2O)_2(MeNO_2)_4]$,[16] and $[Mn_{84}O_{72}(O_2CMe)_{78}(OMe)_{24}(MeOH)_{12}(H_2O)_{42}(OH)_6]$.[17]

A particularly fruitful starting material for a variety of reactions of the second type has been $[Mn_{12}O_{12}(O_2CCH_2Bu^t)_{16}(H_2O)_4]$ (**2**), where $Bu^tCH_2CO_2H$ is 3,3-dimethylbutyric acid (*tert*-butylacetic acid).[16,18,19] For example, the reaction of **2** with MeOH led to the isolation of the novel Mn_{21} cluster $[Mn_{21}O_{24}(OMe)_8(O_2CCH_2Bu^t)_{16}(H_2O)_{10}]$,[18] while reductive destabilization with a reducing agent such as phenol led to the new Mn_8 cluster, $[Mn_8O_2(O_2CCH_2Bu^t)_{14}(HO_2CCH_2Bu^t)_4]$.[19] In addition, the Mn_{30} cluster mentioned above, $[Mn_{30}O_{24}(OH)_8(O_2CCH_2Bu^t)_{32}(H_2O)_2(MeNO_2)_4]$, was obtained by simply recrystallizing **2** from a $CH_2Cl_2/MeNO_2$ solvent mixture.[16] It has been postulated that the strong basicity of the $Bu^tCH_2CO_2^-$ ligand, as reflected in the relatively high pK_a value of its conjugate acid (p$K_a = 5.00$), combined with the bulky and hydrophobic nature of the Bu^t group are the main reasons for the interesting products obtained with this carboxylate.

(1) (a) Sessoli, R.; Tsai, H.-L.; Schake, A. R.; Wang, S.; Vincent, J. B.; Folting, K.; Gatteschi, D.; Christou, G.; Hendrickson, D. N. *J. Am. Chem. Soc.* **1993**, *115*, 1804. (b) Sessoli, R.; Gatteschi, D.; Caneschi, A.; Novak, M. A. *Nature* **1993**, *365*, 141.

(2) (a) Christou, G.; Gatteschi, D.; Hendrickson, D. N.; Sessoli, R. *MRS Bull.* **2000**, *25*, 66. (b) Hill, S.; Edwards, R. S.; Aliaga-Alcalde, N.; Christou, G. *Science* **2003**, *302*, 1015.

(3) (a) Aubin, S. M. J.; Wemple, M. W.; Adams, D. M.; Tsai, H.-L.; Christou, G.; Hendrickson, D. N. *J. Am. Chem. Soc.* **1996**, *118*, 7746. (b) Brockman, J. T.; Abboud, K. A.; Hendrickson, D. N.; Christou, G. *Polyhedron* **2003**, *22*, 1765. (c) Sañudo, E. C.; Brechin, E. K.; Boskovic, C.; Wernsdorfer, W.; Yoo, J.; Yamaguchi, A.; Concolino, T. R.; Abboud, K. A.; Rheingold, A. L.; Ishimoto, H.; Hendrickson, D. N.; Christou, G. *Polyhedron* **2003**, *22*, 2267. (d) Chakov, N. E.; Wernsdorfer, W.; Abboud, K. A.; Christou, G. *Inorg. Chem.* **2004**, *43*, 5919. (e) Mishra, A.; Wernsdorfer, W.; Abboud, K. A.; Christou, G. *J. Am. Chem. Soc.* **2004**, *126*, 15648. (f) Miyasaka, H.; Clérac, R.; Wernsdorfer, W.; Lecren, L.; Bonhomme, C.; Sugiura, K.; Yamashita, M. *Angew. Chem., Int. Ed.* **2004**, *43*, 2801.

(4) (a) Caneschi, A.; Gatteschi, D.; Sessoli, R.; *J. Am. Chem. Soc.* **1991**, *113*, 5873. (b) Wernsdorfer, W.; Aliaga-Alcalde, N.; Hendrickson, D. N.; Christou, G. *Nature* **2002**, *416*, 406.

(5) (a) Eppley, H. J.; Tsai, H.-L.; de Vries, N.; Folting, K.; Christou, G.; Hendrickson, D. N. *J. Am. Chem. Soc.* **1995**, *117*, 301. (b) Eppley, H. J.; Christou, G.; Law, N. A.; Pecoraro, V. L. *Inorg. Synth.* **2002**, *33*, 61.

(6) Soler, M.; Artus, P.; Folting, K.; Huffman, J. C.; Hendrickson, D. N.; Christou, G. *Inorg. Chem.* **2001**, *40*, 4902.

(7) Aubin, S. M. J.; Sun, Z.; Pardi, L.; Krzystek, J.; Folting, K.; Brunel, L.-C.; Rheingold, A. L.; Christou, G.; Hendrickson, D. N. *Inorg. Chem.* **1999**, *38*, 5329.

(8) Schake, A. R.; Tsai, H.-L.; Webb, R. J.; Folting, K.; Christou, G.; Hendrickson, D. N. *Inorg. Chem.* **1994**, *33*, 6020.

(9) Li, J.-Y.; Xu, H.; Zou, J.-Z.; Xu, Z.; You, X.-Z.; Yu, K.-P. *Polyhedron* **1996**, *15*, 3325.

(10) Artus, P.; Boskovic, C.; Yoo, J.; Streib, W. E.; Brunel, L.-C.; Hendrickson, D. N.; Christou, G. *Inorg. Chem.* **2001**, *40*, 4199.

(11) Boskovic, C.; Pink, M.; Huffman, J. C.; Hendrickson, D. N.; Christou, G. *J. Am. Chem. Soc.* **2001**, *123*, 9914.

(12) (a) Chakov, N. E.; Wernsdorfer, W.; Abboud, K. A.; Hendrickson, D. N.; Christou, G. *J. Chem. Soc., Dalton Trans.* **2003**, *11*, 2243. (b) Chakov, N. E.; Abboud, K. A.; Zahkarov, L. N.; Rheingold, A. L.; Hendrickson, D. N.; Christou, G. *Polyhedron* **2003**, *22*, 1759.

(13) (a) Kuroda-Sowa, T.; Fukuda, S.; Miyoshi, S.; Maekawa, M.; Munakata, M.; Miyasaka, H.; Yamashita, M. *Chem. Lett.* **2002,** *31*, 682. (b) Kuroda-Sowa, T.; Handa, T.; Kotera, T.; Maekawa, M.; Munakata, M.; Miyasaka, H.; Yamashita, M. *Chem. Lett.* **2004**, *33*, 540.

(14) (a) Aromí, G.; Aubin, S. M. J.; Bolcar, M. A.; Christou, G.; Eppley, H. J.; Folting, K.; Hendrickson, D. N.; Huffman, J. C.; Squire, R. C.; Tsai, H.-L.; Wang, S.; Wemple, M. W. *Polyhedron* **1998**, *17*, 3005, and refs cited therein. (b) Brechin, E. K.; Yoo, J.; Nakano, M.; Huffman, J. C.; Hendrickson, D. N.; Christou, G. *Chem. Commun.* **1999**, *9*, 783. (c) Boskovic, C.; Brechin, E. K.; Streib, W. E.; Folting, K.; Bollinger, J. C.; Hendrickson, D. N.; Christou, G. *J. Am. Chem. Soc.* **2002**, *124*, 3725. (d) Rajaraman, G.; Murugesu, M.; Sañudo, E. C.; Soler, M.; Wernsdorfer, W.; Helliwell, M.; Muryn, C.; Raftery, J.; Teat, S. J.; Christou, G.; Brechin, E. K. *J. Am. Chem. Soc.* **2004**, *126*, 15445. (e) Murugesu, M.; Raftery, J.; Wernsdorfer, W.; Christou, G.; Brechin, E. K. *Inorg. Chem.* **2004**, *43*, 4203. (f) Murugesu, M.; Wernsdorfer, W.; Abboud, K. A.; Christou, G. *Angew. Chem., Int. Ed.* **2005**, *44*, 892. (g) Foguet-Albiol, D.; O'Brien, T. A.; Wernsdorfer, W.; Moulton, B.; Zaworotko, M. J.; Abboud, K. A.; Christou, G. *Angew. Chem., Int. Ed.* **2005**, *44*, 897.

(15) Soler, M.; Wernsdorfer, W.; Sun, Z.; Huffman, J. C.; Hendrickson, D. N. Christou, G. *Chem. Commun.* **2003**, *21*, 2672.

(16) (a) Soler, M.; Wernsdorfer, W.; Folting, K.; Pink, M.; Christou, G. *J. Am. Chem. Soc.* **2004**, *126*, 2156. (b) Soler, M.; Rumberger, E.; Folting, K.; Hendrickson, D. N.; Christou, G. *Polyhedron* **2001**, *20*, 1365.

(17) Tasiopoulos, A. J.; Vinslava, A.; Wernsdorfer, W.; Abboud, K. A.; Christou, G. *Angew. Chem., Int. Ed.* **2004**, *43*, 2117.

(18) Brockman, J. T.; Huffman, J. C.; Christou, G. *Angew. Chem., Int. Ed.* **2002**, *114*, 2616.

(19) Boskovic, C.; Huffman, J. C.; Christou, G. *Chem. Commun.* **2002**, *21*, 2502.

As part of our continuing interest in SMMs in general and in Mn_{12} complexes in particular, we have extended these investigations of the influence of bulky, hydrophobic groups on the nature of the obtained products. In this paper, we report our findings from the use of the related carboxylic acid 2,2-dimethylbutyric acid (Pe^tCO_2H, where Pe^t is the *tert*-pentyl group, $-CMe_2Et$) with $pK_a = 5.03$, which is similar to $Bu^tCH_2CO_2H$. We herein describe the syntheses, single-crystal X-ray structures, and magnetic properties of the products obtained by the introduction of $Pe^tCO_2^-$ groups into Mn_{12} complexes.

Experimental Section

Syntheses. All manipulations were performed under aerobic conditions using materials as received, except where otherwise noted. $[Mn_{12}O_{12}(O_2CMe)_{16}(H_2O)_4]\cdot 4H_2O\cdot 2MeCO_2H$ (**1**)[20] and $[Mn_{12}O_{12}(O_2CCH_2Bu^t)_{16}(H_2O)_4]$ (**2**)[5a] were prepared as described elsewhere.

$[Mn_{12}O_{12}(O_2CPe^t)_{16}(H_2O)_4]$ (3). A solution of complex **1** (2.0 g, 0.97 mmol) in MeCN (75 cm^3) was treated with a solution of HO_2CPe^t (3.89 cm^3, 31.0 mmol) in CH_2Cl_2 (25 cm^3). The solution was stirred overnight, and the solvent was then removed in vacuo. The residue was dissolved in toluene (20 cm^3), and the solution was again evaporated to dryness. The addition and removal of toluene was repeated two more times. The residue was then dissolved in CH_2Cl_2 (75 cm^3) and treated again with HO_2CPe^t (3.89 cm^3, 31.0 mmol) in CH_2Cl_2 (25 cm^3). After 3 h, three more cycles of addition and removal of toluene were performed. The residue was redissolved in CH_2Cl_2 (50 cm^3), the solution was filtered, and $MeNO_2$ (50 cm^3) was added. The solution was then maintained undisturbed at 4 °C for 4 days. The resulting black crystals were collected by filtration, washed with $MeNO_2$, and dried in vacuo; the yield was ~83%. Anal. Calcd (found) for **3**·CH_2Cl_2 ($C_{97}H_{186}Cl_2O_{48}Mn_{12}$): C, 40.87 (40.78); H, 6.58 (6.53); N, 0.00 (0.00). Selected IR data (cm^{-1}): 1584 (s), 1557 (s), 1524 (s), 1499 (m), 1477 (vs), 1459 (m), 1419 (vs), 1374 (s), 1356 (m), 1326 (m), 1284 (m), 1229 (w), 1209 (m), 1061 (w), 1006 (w), 931 (w), 883 (w), 801 (w), 786 (w), 726 (m), 680 (m), 613 (s), 545 (m), 508 (w), 473 (w), 440 (w).

$[Mn_{12}O_{12}(O_2CPe^t)_{16}(MeOH)_4]$ (4). A solution of complex **3** (0.40 g, 0.14 mmol) in CH_2Cl_2 (20 cm^3) was treated with HO_2CPe^t (2.0 cm^3, 16.0 mmol) and MeOH (10 cm^3). The solution was maintained undisturbed at 4 °C for 6 days. The resulting black crystals were collected by filtration, washed with MeOH, and dried in vacuo; the yield was ~82%. A sample for crystallography was maintained in contact with the mother liquor to prevent the loss of interstitial solvent. Anal. Calcd (found) for **4**·$2CH_2Cl_2$ ($C_{102}H_{196}Cl_4O_{48}Mn_{12}$): C, 40.95 (40.79); H, 6.60 (6.68); N, 0.00 (0.00). Selected IR data (cm^{-1}): 1587 (s), 1559 (s), 1524 (s), 1479 (vs), 1459 (m), 1419 (vs), 1374 (s), 1359 (m), 1324 (m), 1289 (m), 1206 (m), 1179 (m), 1069 (w), 1008 (w), 933 (w), 873 (w), 803 (w), 783 (w), 721 (m), 670 (m), 638 (m), 615 (s), 543 (m), 510 (w), 478 (w), 445 (w).

$[Mn_6O_2(O_2CH_2)(O_2CPe^t)_{11}(HO_2CPe^t)_2(O_2CMe)]$ (5). A solution of complex **3** (0.40 g, 0.14 mmol) in CH_2Cl_2 (20 cm^3) was treated with HO_2CPe^t (2.0 cm^3, 16.0 mmol). The solution was layered with $MeNO_2$ (80 cm^3), and black crystals slowly grew. After 1 week, the crystals were collected by filtration, washed with $MeNO_2$, and dried in vacuo; the yield was ~10%. A sample for crystallography was maintained in contact with the mother liquor to prevent the loss of interstitial solvent. Dried solid appeared to be hygroscopic. Anal. Calcd (found) for **5**·$^1/_2CH_2Cl_2\cdot 4H_2O$ ($C_{81.5}H_{159}Cl_1O_{36}Mn_6$): C, 47.06 (47.09); H, 7.70 (7.73); N, 0.00 (0.11). Selected IR data (cm^{-1}): 1710 (m), 1627 (vs), 1539 (vs), 1477 (vs), 1459 (s), 1437 (m), 1417 (s), 1359 (m), 1326 (w), 1286 (s), 1204 (s), 1066 (m), 1051 (m), 1008 (m), 971 (m), 928 (w), 886 (w), 803 (m), 781 (m), 763 (w), 678 (m), 635 (s), 603 (m), 545 (m), 475 (m), 445 (m).

$[Mn_9O_6(OH)(CO_3)(O_2CPe^t)_{12}(H_2O)_2]$ (6). To a solution of complex **3** (0.40 g, 0.14 mmol) in CH_2Cl_2 (20 cm^3) was added HO_2CPe^t (2.0 cm^3, 16.0 mmol). The solution was layered with $MeNO_2$ (80 cm^3), and black crystals of **5** slowly grew. After 2 weeks, these were removed by filtration through Celite, and the filtrate was evaporated to dryness in vacuo. The residue was redissolved in CH_2Cl_2 (10 cm^3), HO_2CPe^t (1.3 cm^3, 10.0 mmol) was added, and the solution was layered with $MeNO_2$ (40 cm^3). Black crystals slowly grew over 4 weeks, and these were suitable for X-ray studies if maintained in contact with the mother liquor to prevent the loss of interstitial solvent. After 4 weeks, the crystals were isolated by filtration, washed with small volumes of $MeNO_2$, and dried in vacuo; the yield was ~5%. Anal. Calcd (found) for **6**·HO_2CPe^t ($C_{79}H_{149}O_{38}Mn_9$): C, 43.10 (43.16); H, 6.82 (6.77); N, 0.00 (0.02). Selected IR data (cm^{-1}): 1697 (w), 1557 (vs), 1537 (vs), 1474 (vs), 1459 (w), 1419 (vs), 1379 (m), 1364 (m), 1326 (w), 1289 (m), 1204 (m), 1066 (w), 1051 (w), 1006 (w), 808 (w), 783 (w), 690 (w), 665 (w), 653 (w), 613 (m), 413 (w).

$[Mn_4O_2(O_2CPe^t)_6(bpy)_2]$ (7). To a solution of complex **3** (0.25 g, 0.090 mmol) in CH_2Cl_2 (10 cm^3) was added 2,2′-bipyridine (bpy; 0.23 g, 1.4 mmol), and the resulting solution was stirred for 3 h and filtered through Celite. The filtrate was layered with $MeNO_2$ (25 cm^3). Black crystals slowly grew, and these were suitable for X-ray crystallography if maintained in contact with the mother liquor to prevent the loss of interstitial solvent. After 3 days, the crystals were isolated by filtration, washed with $MeNO_2$, and dried in vacuo; the yield was 35%. Anal. Calcd (found) for **7**·$2H_2O$ ($C_{56}H_{86}N_4O_{16}Mn_4$): C, 52.10 (52.17); H, 6.71 (6.65); N, 4.34 (4.34). Selected IR data (cm^{-1}): 1584 (vs), 1547 (s), 1476 (s), 1442 (m), 1420 (vs), 1370 (m), 1357 (m), 1290 (m), 1205 (w), 1161 (w), 1054 (w), 1016 (w), 804(w), 786 (w), 764 (s), 738 (m), 696(m), 653 (m), 630 (s), 415 (m).

$[Mn_9O_7(O_2CCH_2Bu^t)_{13}(THF)_2]$ (8). To a solution of complex **2** (0.20 g, 0.072 mmol) in tetrahydrofuran (THF; 30 cm^3) was added $MeNO_2$ (50 cm^3). The solution was filtered, and the filtrate was allowed to stand undisturbed at 4 °C. Black crystals formed slowly over 2 weeks, and these were suitable for X-ray studies if maintained in contact with the mother liquor to prevent the loss of interstitial solvent. After 2 weeks, the crystals were isolated by filtration, washed with $MeNO_2$, and dried in vacuo; the yield was ~30%. Anal. Calcd (found) for **8**·$^1/_2MeNO_2$ ($C_{86.5}H_{160.5}N_{0.5}O_{36}Mn_9$): C, 45.61 (45.36); H, 7.10 (7.16); N, 0.31 (0.30). Selected IR data (cm^{-1}): 1564 (vs), 1479 (m), 1434 (s), 1409 (vs), 1362 (m), 1306 (w), 1274 (w), 1234 (m), 1196 (w), 1149 (w), 1046 (w), 973 (w), 903 (w), 803 (w), 733 (m), 693 (s), 665 (s), 633 (s), 605 (m), 568 (w), 515 (w), 463 (w).

X-ray Crystallography. Diffraction intensities were collected at 173 K (**4**·2MeCN, **5**·$^1/_2CH_2Cl_2$) and 218 K (**6**·$H_2O\cdot HO_2CPe^t$, **7**·$2H_2O$), respectively, with a Bruker SMART 1000 and a Bruker P3 diffractometer equipped with a CCD area detector and a graphite monochromator utilizing Mo Kα radiation ($\lambda = 0.710\ 73$ Å). The crystallographic data and details of the X-ray studies are collected in Table 1. Space groups were determined on the basis of systematic absences (**5**, **7**), intensity statistics (**4**), or both (**6**). Absorption corrections were applied on the basis of measured indexed crystal faces (**4**, **5**) and by SADABS (**6**, **7**). Structures were solved by

(20) Lis, T. *Acta Crystallogr.* **1980**, *B36*, 2042.

Table 1. Crystallographic Data for Complexes **4**·2MeCN, **5**·$^1/_2CH_2Cl_2$, **6**·H_2O·HO_2CPe^t and **7**·$2H_2O$

	4	**5**	**6**	**7**
formula[a]	$C_{104}H_{198}N_2Mn_{12}O_{48}$	$C_{81.5}H_{151}Cl_1Mn_6O_{32}$	$C_{79}H_{151}Mn_9O_{39}$	$C_{56}H_{86}N_4Mn_4O_{16}$
fw, g mol^{-1}	2903.96	2008.16	2219.49	1291.07
space group	$P\bar{1}$	$P2_1/c$	$Cmc2_1$	$P2_1/c$
a, Å	16.285(3)	15.980(2)	25.9274(14)	12.9936(10)
b, Å	16.556(3)	21.255(3)	19.6851(10)	18.8216(14)
c, Å	27.839(5)	30.570(4)	21.1978(12)	14.0822(10)
α, deg	83.524(3)	90	90	90
β, deg	74.242(3)	101.675(2)	90	107.1740(10)
γ, deg	70.340(3)	90	90	90
V, Å^3	6801(2)	10168(2)	10819(1)	3290.4(4)
Z	2	4	4	4
T, °C	−100(2)	−100(2)	−55(2)	−55(2)
radiation,[b] Å	0.710 73	0.071 073	0.710 73	0.710 73
ρ_{calc}, g cm^{-3}	1.404	1.309	1.356	1.339
μ, cm^{-1}	11.51	8.21	10.89	8.17
R1 (wR2),[c,d] %	8.36 (19.93)	6.97 (17.69)	6.59 (18.05)	5.30 (15.42)

[a] Including solvent molecules. [b] Graphite monochromator. [c] $R1 = \Sigma||F_o| - |F_c||/\Sigma|F_o|$. [d] $wR2 = [\Sigma[w(F_o^2 - F_c^2)^2]/\Sigma[wF_o^2)^2]]^{1/2}$, where $S = [\Sigma[w(F_o^2 - F_c^2)^2]/(n-p)]^{1/2}$, $w = 1/[\sigma^2(F_o^2) + (mp)^2 + np]$, $p = [\max(F_o^2,0) + 2F_c^2]/3$, and *m* and *n* are constants.

direct methods and standard Fourier techniques, and they were refined on F^2 using full matrix least-squares procedures.

The MeCN molecules in **4** and the HO_2CPe^t group in **6** are disordered, and they were treated by the SQUEEZE[21] program, a part of the PLATON package of crystallographic software; the correction of the X-ray data was 361 electrons/cell, and the required value is 256 electrons/cell (**6**). A common feature in each of the structures is a disorder of Me and Et groups in some bridging *tert*-pentylate groups. The Me and Et groups are disordered in six groups in **4**, seven groups in **5**, and two groups in **6** and **7**. Additionally, the Me group of the MeOH ligand coordinated to Mn(12) in **4** was disordered over two positions [C(14) and C(15)], and the occupancies refined to 61:39%. The models for these disorders included refinements over two sites with correlated site occupation factors. Non-hydrogen atoms were refined anisotropically, except those of disordered groups, which were refined with isotropic thermal parameters. In **6**, all carbon atoms in the Pe^t groups were refined with isotropic thermal parameters. Hydrogen atoms were placed in calculated positions and refined with a riding group model. The H atoms in some highly disordered groups, solvent water molecules, and the OH^- group in **6** were not included. Restrictions for the C−C distances in ligands were used in the refinement of **6**. The non-centrosymmetric crystal of **6** was treated as a racemic twin; the Flack parameter is 0.52(2). Maximum and minimum peaks on the residual densities in **4**−**7** are in the range between +1.093 and −0.643 e Å^{-3}.

Other Studies. Infrared spectra were recorded in the solid state (KBr pellets) on a Nicolet Nexus 670 FTIR spectrophotometer in the 400−4000 cm^{-1} range. Elemental analyses (C, H, and N) were performed at the in-house facilities of the University of Florida Chemistry Department. Electrochemical studies were performed under argon using a BAS model CV-50W voltammetric analyzer and a standard three-electrode assembly (glassy carbon working, Pt wire auxiliary, and Ag/Ag_3I_4 reference) with 0.1 M $NBu^n_4PF_6$ as supporting electrolyte. No IR compensation was employed. Quoted potentials are vs ferrocene, used as an internal standard. The scan rates for cyclic voltammetry (CV) and differential pulse voltammetry (DPV) were 100 and 20 mV/s, respectively. Distilled solvents were employed, and the concentrations of the complexes were approximately 1 mM. Variable-temperature DC magnetic susceptibility data down to 1.80 K were collected on a Quantum Design MPMS-XL SQUID magnetometer equipped with a 70 kG (7 T) DC magnet at the University of Florida. Pascal's constants were used to estimate the diamagnetic corrections, which were subtracted from the experimental susceptibility to give the molar magnetic susceptibility (χ_M). AC magnetic susceptibility data were collected on the same instrument employing a 3.5 G field oscillating at frequencies up to 1500 Hz.

(21) Van der Sluis, P.; Spek, A. L. *Acta Crystallogr.* **1990**, *A46*, 194.

Results and Discussion

Syntheses. To introduce the hydrophobic $Pe^tCO_2^-$ group onto the Mn_{12} core, we employed the previously developed carboxylate substitution reaction that involves the treatment of $[Mn_{12}O_{12}(O_2CMe)_{16}(H_2O)_4]$·$4H_2O$·$2MeCO_2H$ with an excess of RCO_2H.[5] Thus, a solution of complex **1** in MeCN was treated with an excess of Pe^tCO_2H in CH_2Cl_2. The reaction is an equilibrium that was driven to completion by several cycles of removal of acetic acid as its toluene azeotrope (28:72%; bp 101 °C at 1 atm) under reduced pressure (eq 1). The product was subsequently crystallized with $MeNO_2$ and identified by infrared spectroscopy and elemental analysis as $[Mn_{12}O_{12}(O_2CPe^t)_{16}(H_2O)_4]$ (**3**).

$$[Mn_{12}O_{12}(O_2CMe)_{16}(H_2O)_4] + 16\ Pe^tCO_2H \rightarrow [Mn_{12}O_{12}(O_2CPe^t)_{16}(H_2O)_4] + 16\ MeCO_2H \quad (1)$$

The stability of complex **3** to recrystallization from $CH_2Cl_2/MeNO_2$ or CH_2Cl_2/MeOH was investigated both in the presence and absence of the free carboxylic acid. We had previously observed[15] that $[Mn_{12}O_{12}(O_2CCH_2Bu^t)_{16}(H_2O)_4]$ (**2**) can be recrystallized without change from these solvent systems in the presence of $Bu^tCH_2CO_2H$. However, in the absence of the latter, the Mn_{30} and Mn_{21} clusters, respectively, mentioned earlier were obtained.[16,18] Somewhat different results were obtained with **3**: in the presence of Pe^tCO_2H, recrystallization from CH_2Cl_2/MeOH and $CH_2Cl_2/MeNO_2$ gave $[Mn_{12}O_{12}(O_2CPe^t)_{16}(MeOH)_4]$ (**4**) and $[Mn_6O_2(O_2CH_2)(O_2CPe^t)_{11}(HO_2CPe^t)_2(O_2CMe)]$ (**5**), respectively. In the absence of Pe^tCO_2H, each recrystallization gave materials that, by infrared spectroscopy and elemental analysis, have not retained the Mn_{12} core but that are not **4** or **5**. However, we have been unable to date to identify these products.

The crystallization solutions from the reaction of **3** with Pe^tCO_2H in a solvent mixture of $CH_2Cl_2/MeNO_2$ were allowed to stand for several weeks in an effort to increase the yield of complex **5**, a new structural type. Instead, several products crystallized, including complexes **3** and **5** and a number of other materials. The reaction system is unquestionably very complicated, with several species no doubt in equilibrium in solution. The initial crystalline products were separated by filtration, the filtrate concentrated to dryness by rotoevaporation, a small amount of Pe^tCO_2H added to the residue, and the latter dissolved in CH_2Cl_2. Layering the solution with $MeNO_2$ slowly gave small crystals of $[Mn_9O_6(OH)(CO_3)(O_2CPe^t)_{12}(H_2O)_2]$ (**6**) containing a bridging CO_3^{2-} group. This was an unexpected result that can be rationalized by reasoning that the CO_3^{2-} ligand in **6** likely arises from the oxidation of the $O_2CH_2^{2-}$ ligand in **5**, which itself likely originates from the oxidation of CH_2Cl_2, a process for which there is precedent in the literature.[22] Alternatively, the CO_3^{2-} ligand in **6** may be from the reaction of **5** with atmospheric CO_2, as has been previously observed with a series of hydroxo complexes $[M(HB(3,5\text{-}^iPr_2pz)_3)]_2(OH)_2$ ($HB(3,5\text{-}^iPr_2pz)_3$ = hydrotris(3,5-diisopropyl-1-pyrazolyl)borate and M = Mn^{II}, Fe^{II}, Co^{II}, Ni^{II}, Cu^{II}, and Zn^{II}).[23] Although mechanistic studies are not feasible for this complicated reaction system, it can be noted that neither complexes **5** nor **6** crystallize from identical reactions carried out in $CHCl_3$ instead of CH_2Cl_2. In addition, the infrared spectra of materials obtained from similar reactions using $[Mn_{12}O_{12}(O_2CBu^t)_{16}(H_2O)_4]$ and Bu^tCO_2H suggest that structural analogues of complexes **5** or **6** are not obtained. Although these results support the suggestion that the $O_2CH_2^{2-}$ and CO_3^{2-} ligands originate from CH_2Cl_2 and not atmospheric CO_2 or carboxylate groups, the exact mechanism remains unclear.

We also investigated the reactivity of the Pe^t-substituted Mn_{12} cluster **3** under the various conditions explored earlier for the $Bu^tCH_2CO_2^-$-substituted derivative (**2**), specifically with chelates and reducing agents. Reactions of complex **3** with 2,6-pyridinedimethanol ($pdmH_2$), 2,2′-bipyridine (bpy), and phenol were carried out in CH_2Cl_2. Large crystals of $[Mn_4O_2(O_2CPe^t)_6(bpy)_2]$ (**7**) were obtained in high yield from the reaction of **3** with bpy. IR spectra of the solids obtained from reactions with either $pdmH_2$ or phenol suggested the product to be $[Mn_8O_2(O_2CPe^t)_{14}(HO_2CPe^t)_4]$, the Pe^t analogue of $[Mn_8O_2(O_2CCH_2Bu^t)_{14}(HO_2CCH_2Bu^t)_4]$[19] mentioned in the Introduction. However, not enough material was isolated from these reactions for more definitive characterization. To further understand the reaction system, recrystallization was explored of complexes **2** and **3** from solvent mixtures other than $CH_2Cl_2/MeNO_2$, in the absence of the corresponding acid. As mentioned earlier, the Mn_{30} complex was obtained by dissolution of complex **2** in this mixture of solvents; in fact, this transformation to Mn_{30} requires the presence of $MeNO_2$. Hence, several solvents were explored in place of the CH_2Cl_2, and among these was tetrahydrofuran (THF). Indeed, we obtained black needlelike crystals from a dark brown solution of **2** in THF/$MeNO_2$. Preliminary X-ray analysis identified the product as $[Mn_9O_7(O_2CCH_2Bu^t)_{16}(THF)_2]$ (**8**), but we have been unable to obtain suitable crystals for a high-quality structure refinement. The transformation of **2** into **8** is summarized in

$$[Mn_{12}O_{12}(O_2CCH_2Bu^t)_{16}(H_2O)_4] + 2THF + H^+ + 4e^- \rightleftharpoons [Mn_9O_7(O_2CCH_2Bu^t)_{13}(THF)_2] + 3Mn^{3+} + 3Bu^tCH_2CO_2^- + 9OH^- \quad (2)$$

The average oxidation state of the starting material is +3.33, while that of the product (**8**) is only +3. Thus, the formation of complex **8** appears to involve the reduction of **2** followed by structural rearrangement.

Electrochemistry. Previous studies have established the Mn_{12} clusters to exhibit interesting electrochemical behavior.[5a,24] They normally display several oxidation and reduction processes of which at least one reduction wave is usually reversible by the usual electrochemical standards (cyclic voltammogram (CV) peak separations, differential pulse voltammogram (DPV) peak broadness, $i_{anodic}/i_{cathodic}$ peak current ratio, and linearity of peak current vs $v^{1/2}$ plots, where v is the scan rate). In addition, as expected the redox processes are very sensitive to the electron-withdrawing or -donating ability of the carboxylate ligand, and we have reported the $E_{1/2}$ values for a number of Mn_{12} derivatives. The range of $E_{1/2}$ values (vs Fc/Fc^+) for the first one-electron reduction ranges from +0.91 V for the R = $CHCl_2$ complex to 0.00 V for the R = *p*-C_6H_4OMe complex. Similarly, the second reduction ranges from +0.61 V for the R = $CHCl_2$ complex to −0.50 V for the R = Et complex. The potential of the first oxidation process varies from 1.07 V for R = $C_6H_4CF_3$ to 0.70 V for R = *p*-C_6H_4OMe or *p*-C_6H_4Et. By reduction with either 1 or 2 equiv of I^-, both the one- and two-electron reduced forms of some Mn_{12} species have been isolated and structurally characterized (I^-/I_2 couple occurs at 0.21 V in CH_2Cl_2 vs Fc/Fc^+).[5a,24] However, despite the reversible nature of the oxidation processes of several characterized Mn_{12} clusters, a one-electron oxidized Mn_{12} cluster has not yet been isolated. This is likely due in part to the high potentials associated with this process. The introduction of a strongly electron donating ligand onto the Mn_{12} complex would likely make more feasible the preparation of a one-electron oxidized Mn_{12} derivative by moving the first oxidation process to more accessible potentials, and we decided to explore this.

The cyclic voltammogram and differential pulse voltammogram of **4** are shown in Figure 1. There is a quasireversible oxidation wave at −0.21 V and an irreversible reduction wave at −0.87 V. The CV and DPV profiles of **2** are very similar; a quasireversible oxidation wave occurs at −0.07 V and an irreversible reduction appears at −0.82

(22) Scherer, O. J.; Jungmann, H.; Hussong, K. *J. Organomet. Chem.* **1983**, *247*, C1.
(23) Kitajima, N.; Hikichi, S.; Tanaka, M.; Moro-oka, Y. *J. Am. Chem. Soc.* **1993**, *115*, 5496.
(24) Soler, M.; Wernsdorfer, W.; Abboud, K. A.; Huffman, J. C.; Davidson, E. R.; Hendrickson, D. N.; Christou, G. *J. Am. Chem. Soc.* **2003**, *125*, 3576.

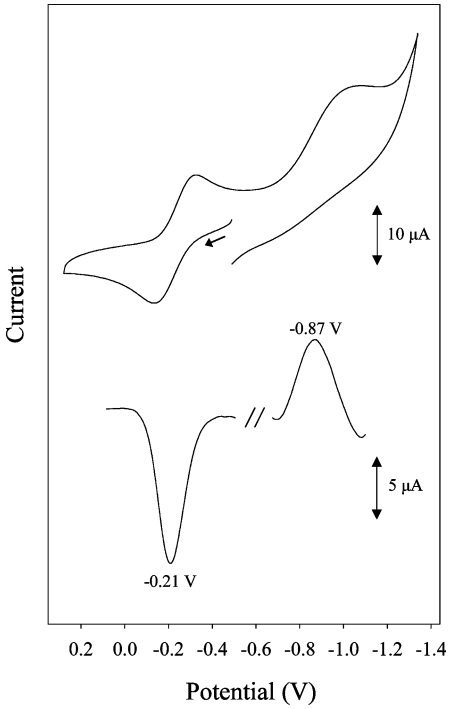

Figure 1. Cyclic voltammogram at 100 mV s^{-1} (top) and differential pulse voltammogram (bottom) at 20 mV s^{-1} for complex **4** in CH_2Cl_2 containing 0.1 M $NBu^n_4PF_6$ as supporting electrolyte. The indicated potentials are vs Fc/Fc^+.

V. The oxidation processes of both complexes meet the standard electrochemical requirements for quasireversible electron transfer. A study of υ dependence for the oxidation waves showed a linear dependence of peak current with respect to $\upsilon^{1/2}$, indicating that the process is diffusion-controlled.

X-ray Crystal Structures. A labeled ORTEP[25] plot in PovRay format of complex **4** is shown in Figure 2, together with a stereoview. Selected interatomic distances are listed in Table 2. The complex crystallizes in the triclinic space group $P\bar{1}$ with the asymmetric unit consisting of the Mn_{12} molecule and two MeCN molecules of crystallization. The structure of **4** is very similar to other previously characterized neutral Mn_{12} complexes,[1a,5a] consisting of a central $[Mn^{IV}_4O_4]$ cubane that is surrounded by a nonplanar ring of eight Mn^{III} atoms that are bridged and connected to the cubane by eight μ_3-O^{2-} ions. The eight Mn^{III} ions separate into two groups of four Mn^{III} ions each. In the first group, each Mn^{III} ion is coordinated to a single Mn^{IV} ion via two oxide bridges [Mn(5), Mn(7), Mn(9), Mn(11)], while in the second group each Mn^{III} ion is coordinated to two Mn^{IV} ions via two oxide bridges [Mn(6), Mn(8), Mn(10), Mn(12)].[26] Peripheral ligation is by sixteen bridging $Pe^tCO_2^-$ ligands and four terminal MeOH groups, which are bound in a 1:1:2 fashion to Mn(8), Mn(10), and Mn(12), respectively (Figure 2). The oxidation levels of the Mn ions were assigned by analysis

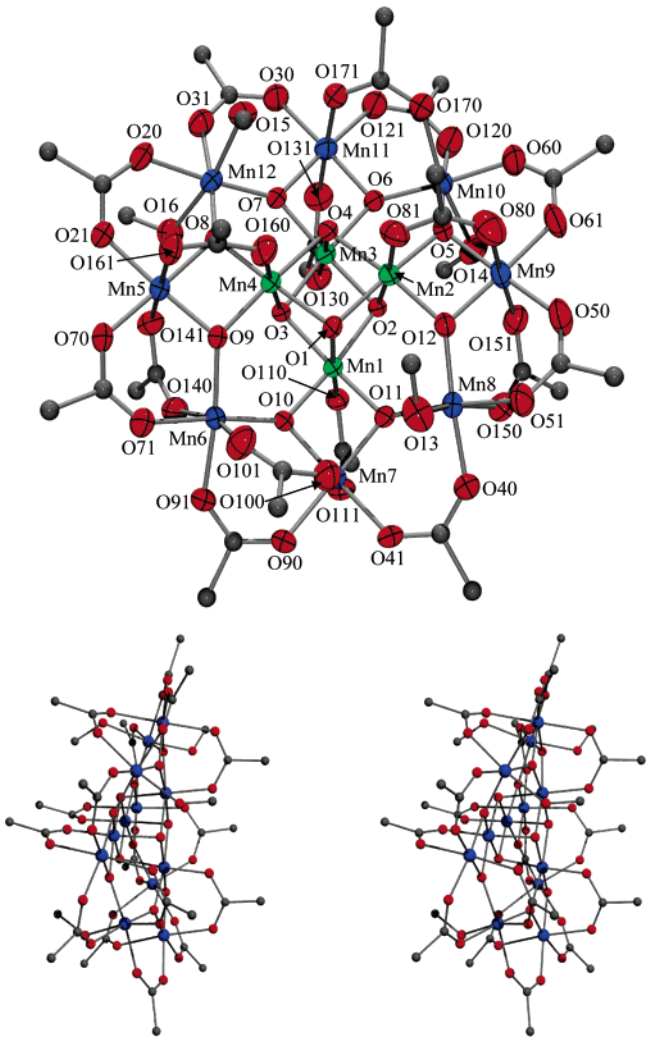

Figure 2. ORTEP representation in PovRay format of complex **4** at the 50% probability level, together with a stereopair. For clarity, the hydrogen atoms have been omitted, and only the quaternary C atoms of the ligands are shown: Mn^{IV}, green; Mn^{III}, blue; O, red; C, gray.

of the Mn−O bond distances, charge considerations, and bond valence sum (BVS) calculations.[27] As expected, each of the Mn^{III} ions exhibits Jahn−Teller (JT) elongation of two trans bonds, as expected for a high-spin d^4 ion in near-octahedral geometry. The JT elongation axes of the eight Mn^{III} ions of the outer ring are aligned approximately parallel to each other, roughly perpendicular to the $[Mn_{12}O_{12}]$ disklike core of the molecule (Figure 3).

In addition to sixteen bridging carboxylate ligands, either three or four water molecules are coordinated to the four Mn^{III} ions in the second group described above [Mn(6), Mn(8), Mn(10), Mn(12)],[28] in all but two of the previously characterized Mn_{12} complexes; the exceptions are the $[Mn_{12}O_{12}(O_2CMe)_{12}(dpp)_4]$ complex in which there are four five-coordinate Mn^{III} centers and no coordinating water molecules[29] and the $[Mn_{12}O_{12}(O_2CMe)_{16}(MeOH)_4]$ complex in which there are four coodinated MeOH ligands.[30] Both

(25) Johnson, C. K.; Burnett, M. N. *ORTEP−III*; Report ORNL-6895; Oak Ridge National Laboratory: Oak Ridge, TN, 1996. Farrugia, L. J. *J. Appl. Crystallogr.* **1997**, *30*, 565.
(26) Ruiz, D.; Aubin, S. M. J.; Rumberger, E.; Incarvito, C. D.; Folting, K.; Rheingold, A. L.; Christou, G.; Hendrickson, D. N. *Mol. Cryst. Liq. Cryst.* **1999**, *335*, 413.
(27) (a) Brown, I. D.; Wu, K. K. *Acta Crystallogr.* **1976**, *B32*, 1957. (b) Palenik, G. J. *Inorg. Chem.* **1997**, *36*, 4888.
(28) Aubin, S. M. J.; Ruiz, D.; Rumberger, E.; Sun, Z.; Albela, B.; Wemple, M. W.; Dilley, N. R.; Ribas, J.; Maple, M. B.; Christou, G.; Hendrickson, D. N. *Mol. Cryst. Liq. Cryst.* **1999**, *335*, 371.

Table 2. Selected Bond Distances[a] (Å) for Complex **4**

Mn(1)−O(10)	1.870(4)	Mn(6)−O(9)	1.893(4)
Mn(1)−O(11)	1.879(4)	Mn(6)−O(91)	1.964(5)
Mn(1)−O(1)	1.913(4)	Mn(6)−O(71)	1.972(5)
Mn(1)−O(110)	1.913(5)	Mn(6)−O(140)	2.150(6)
Mn(1)−O(2)	1.921(4)	Mn(6)−O(101)	2.168(6)
Mn(1)−O(3)	1.940(4)	Mn(7)−O(10)	1.898(4)
Mn(1)···Mn(7)	2.7873(14)	Mn(7)−O(11)	1.916(4)
Mn(1)···Mn(4)	2.8263(14)	Mn(7)−O(41)	1.942(5)
Mn(1)···Mn(2)	2.8399(14)	Mn(7)−O(90)	1.956(5)
Mn(1)···Mn(3)	2.9656(14)	Mn(7)−O(100)	2.153(6)
Mn(2)−O(12)	1.860(4)	Mn(7)−O(111)	2.162(5)
Mn(2)−O(5)	1.883(4)	Mn(8)−O(12)	1.870(4)
Mn(2)−O(4)	1.908(4)	Mn(8)−O(11)	1.904(4)
Mn(2)−O(2)	1.912(4)	Mn(8)−O(40)	1.930(5)
Mn(2)−O(81)	1.930(5)	Mn(8)−O(51)	1.988(5)
Mn(2)−O(1)	1.934(4)	Mn(8)−O(150)	2.156(6)
Mn(2)−Mn(9)	2.7914(15)	Mn(8)−O(13)	2.239(6)
Mn(2)−Mn(3)	2.8348(16)	Mn(9)−O(5)	1.897(5)
Mn(2)−Mn(4)	2.9421(14)	Mn(9)−O(12)	1.898(4)
Mn(3)−O(6)	1.869(4)	Mn(9)−O(61)	1.930(5)
Mn(3)−O(7)	1.894(4)	Mn(9)−O(50)	1.960(6)
Mn(3)−O(4)	1.898(5)	Mn(9)−O(151)	2.160(6)
Mn(3)−O(3)	1.914(4)	Mn(9)−O(80)	2.191(7)
Mn(3)−O(2)	1.939(4)	Mn(10)−O(6)	1.877(5)
Mn(3)−O(130)	1.940(5)	Mn(10)−O(5)	1.886(5)
Mn(3)−Mn(11)	2.7920(15)	Mn(10)−O(60)	1.949(6)
Mn(3)−Mn(4)	2.8265(15)	Mn(10)−O(120)	1.970(6)
Mn(4)−O(8)	1.869(4)	Mn(10)−O(170)	2.138(6)
Mn(4)−O(9)	1.873(4)	Mn(10)−O(14)	2.241(6)
Mn(4)−O(3)	1.901(5)	Mn(11)−O(6)	1.885(4)
Mn(4)−O(1)	1.903(4)	Mn(11)−O(7)	1.915(5)
Mn(4)−O(160)	1.918(5)	Mn(11)−O(30)	1.941(5)
Mn(4)−O(4)	1.939(4)	Mn(11)−O(121)	1.951(5)
Mn(4)···Mn(5)	2.7699(15)	Mn(11)−O(171)	2.156(6)
Mn(5)−O(9)	1.886(4)	Mn(11)−O(131)	2.162(6)
Mn(5)−O(8)	1.903(4)	Mn(12)−O(7)	1.872(5)
Mn(5)−O(70)	1.931(5)	Mn(12)−O(8)	1.873(5)
Mn(5)−O(21)	1.951(5)	Mn(12)−O(31)	1.969(5)
Mn(5)−O(141)	2.165(6)	Mn(12)−O(20)	1.978(5)
Mn(5)−O(161)	2.214(6)	Mn(12)−O(15)	2.208(6)
Mn(6)−O(10)	1.886(4)	Mn(12)−O(16)	2.211(5)

[a] Full listings in the Supporting Information.

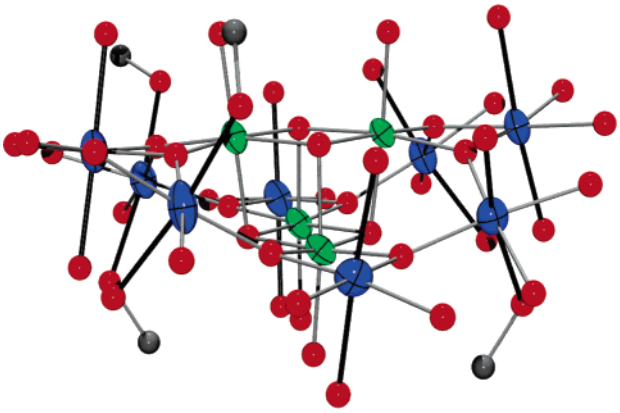

Figure 3. $[Mn_{12}O_{44}(MeOH)_4]$ core of complex **4**, emphasizing the relative disposition of the Jahn−Teller elongation axes indicated as solid black bonds.

complexes have been only recently reported. Instead of water ligands, complex **4** has four MeOH ligands coordinated to the three Mn^{III} ions of the second group [O(13) to Mn(8),

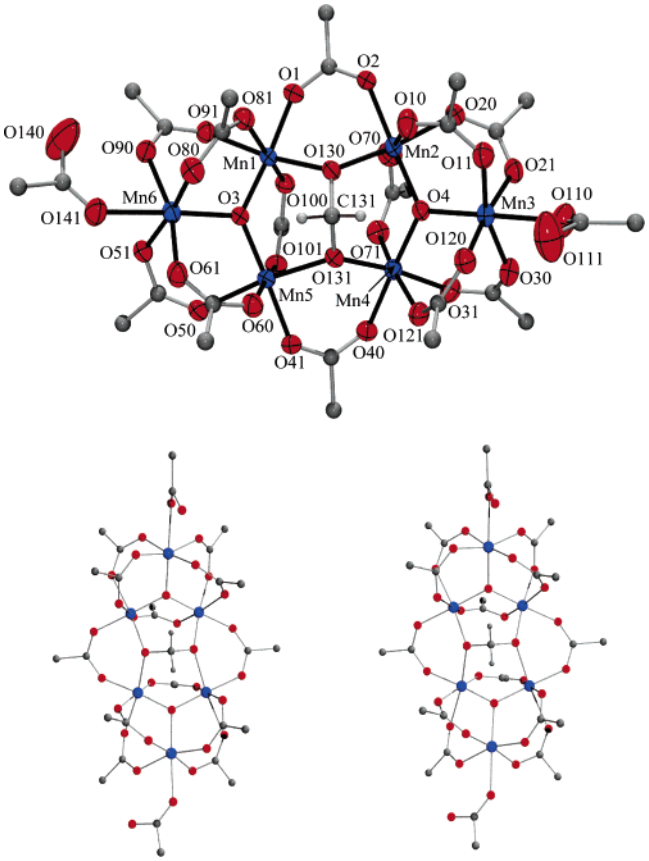

Figure 4. ORTEP representation in PovRay format of complex **5** at the 50% probability level, together with a stereopair. For clarity, the hydrogen atoms have been omitted, and only the quaternary C atoms of the ligands are shown: Mn^{III}, blue; O, red; C, gray.

O(14) to Mn(10), O(15) and O(16) to Mn(12)]. This 1:1:2 ligand distribution pattern has also been observed for $[Mn_{12}O_{12}(O_2CC_6H_4\text{-}p\text{-}Me)_{16}(H_2O)_4]\cdot 3H_2O$.[26,28,31]

The Mn_{12} molecules in the triclinic $P\bar{1}$ lattice are stacked in columns along the *b* axis of the crystal; all of the molecules are oriented in the same manner with respect to the cell axes. The disordered Pe^t groups encapsulate the $[Mn_{12}O_{12}]^{16+}$ core of **4**, clearly separating individual Mn_{12} molecules from their neighbors. Similarly, Bu^t groups have been found to result in the same separation between molecules in other Mn aggregates with ligation by $Bu^tCH_2CO_2^-$.[15,16] Hence, there is no evidence of intermolecular interactions in **4**. Disordered MeCN solvent molecules of crystallization are situated in the large voids separating the columns although their clear visualization is precluded by the use of the program SQUEEZE[21] to remove their overall electron density as discussed in the Experimental Section.

A labeled ORTEP[25] plot in PovRay format of complex **5** is shown in Figure 4, together with a stereoview. Selected interatomic distances and angles are listed in Table 3. The complex crystallizes in the monoclinic space group $P2_1/c$ with the Mn_6 molecule in a general position. The structure consists of a $[Mn^{III}_6(\mu_3\text{-}O)_2(\mu_4\text{-}O_2CH_2)]^{12+}$ core (Figure 5) with the peripheral ligation provided by eleven bridging

(29) Bian, G.-Q.; Kuroda-Sowa, T.; Konaka, H.; Hatano, M.; Maekawa, M.; Munakata, M.; Miyasaka, H.; Yamashita, M. *Inorg. Chem.* **2004**, *43*, 4790.
(30) Bian, G.-Q.; Kuroda-Sowa, T.; Gunjima, N.; Maekawa, M.; Munakata, M. *Inorg. Chem. Commun.* **2005**, *8*, 208.
(31) Aubin, S. M. J.; Sun, Z.; Eppley, H. J.; Rumberger, E. M.; Guzei, I. A.; Folting, K.; Gantzel, P. K.; Rheingold, A. L.; Christou, G.; Hendrickson, D. N. *Inorg. Chem.* **2001**, *40*, 2127.

Table 3. Selected Distances (Å) and Angles[a] (deg) for Complex **5**

Mn(1)−O(3)	1.838(3)	Mn(4)−O(4)	1.866(3)
Mn(1)−O(1)	1.934(3)	Mn(4)−O(131)	1.903(3)
Mn(1)−O(100)	1.997(3)	Mn(4)−O(40)	1.963(4)
Mn(1)−O(81)	2.055(4)	Mn(4)−O(31)	1.966(4)
Mn(1)−O(130)	2.088(3)	Mn(4)−O(121)	2.216(4)
Mn(1)−O(91)	2.152(4)	Mn(4)−O(71)	2.231(4)
Mn(2)−O(4)	1.856(3)	Mn(5)−O(3)	1.850(3)
Mn(2)−O(130)	1.913(3)	Mn(5)−O(41)	1.931(4)
Mn(2)−O(2)	1.948(4)	Mn(5)−O(101)	1.956(4)
Mn(2)−O(20)	1.996(4)	Mn(5)−O(60)	2.017(4)
Mn(2)−O(10)	2.173(4)	Mn(5)−O(131)	2.128(3)
Mn(2)−O(70)	2.211(4)	Mn(5)−O(50)	2.176(4)
Mn(3)−O(21)	1.935(4)	Mn(6)−O(51)	1.903(4)
Mn(3)−O(30)	1.947(4)	Mn(6)−O(80)	1.923(4)
Mn(3)−O(120)	1.947(4)	Mn(6)−O(61)	1.955(4)
Mn(3)−O(11)	1.982(4)	Mn(6)−O(90)	1.981(4)
Mn(3)−O(4)	2.015(3)	Mn(6)−O(3)	2.065(3)
Mn(3)−O(110)	2.277(5)	Mn(6)−O(141)	2.323(4)
Mn(2)−O(130)−Mn(1)	126.61(17)	Mn(4)−O(131)−Mn(5)	126.40(17)

[a] Full listings in the Supporting Information.

$Pe^tCO_2^-$ ligands, one bridging $MeCO_2^-$ ligand, and two terminal Pe^tCO_2H ligands. Bond valence sum calculations[27] indicate that all of the distorted octahedral Mn centers are at the +3 oxidation level.

The six manganese ions are arranged in a twisted boat conformation, which can be described as two trinuclear $[Mn_3(\mu_3\text{-}O)]^{7+}$ units linked at one of their edges by two μ-$Pe^tCO_2^-$ and one μ_4-$O_2CH_2^{2-}$ groups. The dihedral angle between the Mn(2)−Mn(3)−Mn(4) and Mn(1)−Mn(5)−Mn(6) planes is 57.0°. The central μ_3-O^{2-} ion O(3) in one triangular unit is slightly (0.04 Å) out of the Mn_3 plane that it bridges [Mn(1), Mn(5), and Mn(6)]. The other μ_3-O^{2-} ion O(4) is essentially coplanar with the three Mn centers [Mn(2), Mn(3), and Mn(4)].

The remaining two Mn_2 edges within each triangular unit are bridged by two μ-$Pe^tCO_2^-$ groups. There is an additional $Pe^tCO_2^-$ group bridging Mn(1) and Mn(5), but the corresponding pair Mn(2) and Mn(4) in the other triangular unit is bridged by an acetate group. Peripheral ligation at both Mn(3) and Mn(6) is completed by two monodentate Pe^tCO_2H groups. The Mn−O(3) and Mn−O(4) bond distances and Mn−O(3)−Mn and Mn−O(4)−Mn angles within each triangular unit are inequivalent, and the triangles are thus scalene. Only two other examples of a μ_4-$O_2CH_2^{2-}$ bridging unit as found in **5** have been previously observed in the compounds $(NBu^n_4)[Mo_4O_{12}(OH)(O_2CH_2)]$ and in $[Fe_6O_2(O_2CH_2)(O_2CCH_2Bu^t)_{12}(py)_2]$,[33] a compound very similar to **5**. Complexes containing somewhat similar bridging motifs include $Na[Fe_4(dhpta)_2(\mu\text{-}O)(\mu\text{-}OH)(\mu\text{-}ala)_2]$ and $[Mn_4(dhpta)_2(\mu\text{-}O)(\mu\text{-}OH)(\mu\text{-}O_2CMe)_2]^{4-}$ (H_5dhpta = 2-hydroxytrimethylenedinitriloacetic acid and ala = alanine), where either four Fe or Mn ions are bridged by a hydrogen-bonded $O^{2-}\cdots HO^-$ unit rather than a single diolate unit as in **5**.[34,35] The overall

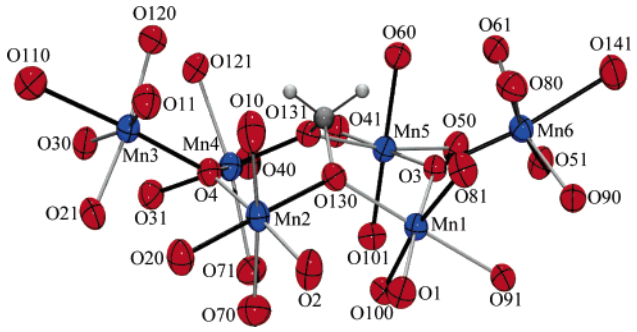

Figure 5. $[Mn_6O_{30}CH_2]$ core of complex **5**, emphasizing the relative disposition of the Jahn−Teller elongation axes indicated as solid black bonds.

structure of **5** as two M_3 triangular units linked at one edge has not been seen before in Mn chemistry, although it is commonly encountered in Fe chemistry.[36−39]

Each of the octahedral Mn^{III} centers in **5** displays a JT axial elongation (Figure 5). Normally, JT elongation axes avoid Mn−oxide bonds, almost always the strongest and shortest in the molecule, but in the case of Mn(3) and Mn(6) the JT elongation axis is situated in an abnormal position containing a core O^{2-} ion, O(4) and O(3), respectively. The JT elongation axes of Mn(2) and Mn(4) are oriented nearly parallel to each other along Mn−O(carboxylate) bonds. In addition, the JT elongation axes of Mn(1) and Mn(5) are along Mn−O(carboxylate) and Mn−O(gem-diolate) bonds and are almost parallel to each other, but essentially perpendicular to those of Mn(2) and Mn(4). This will be of relevance to the magnetic discussion later (vide infra).

A labeled ORTEP[25] plot in PovRay format of complex **6** is shown in Figure 6, together with a stereoview. Selected interatomic distances and angles are listed in Table 4. Complex **6** has crystallographic C_s symmetry, the mirror plane containing Mn(1), Mn(2) and Mn(3). The structure consists of a $[Mn^{III}_9(\mu_3\text{-}O)_6(\mu\text{-}OH)(\mu_3\text{-}CO_3)]^{12+}$ core with peripheral ligation provided by twelve bridging $Pe^tCO_2^-$ ligands and two terminal water molecules. The base of the $[Mn_9O_6(OH)(CO_3)]$ core may be viewed as containing a $[Mn_7O_4]$ subunit consisting of two $[Mn_4O_2]$ "butterfly" units [atoms Mn(1), Mn(2), Mn(4), Mn(4a) and Mn(2), Mn(3), Mn(5), Mn(5a)] fused at five-coordinate Mn(2). These two fused butterfly units form a basketlike subunit of the molecule. The resultant $[Mn_3O_4]$ base of the basket [Mn(1), Mn(2), Mn(3), O(1), O(2)] is not planar but bent with Mn(1)−Mn(2)-Mn(3) = 169.1°. The remaining two Mn atoms, Mn(6) and Mn(6a), represent the "handle" of the basket and are connected to the fused-butterfly unit by a $\eta^1,\eta^1,\eta^1,\mu_3$-$CO_3^{2-}$ group through atoms O(5), O(6), and O(6a) and two μ_3-O^{2-} ions [O(3) and O(3a)]. One OH^- ion [O(4)] and one carboxylate ligand bridge Mn(6) and Mn(6a) across the

(32) Day, V. W.; Fredrich, M. F.; Klemperer, W. G.; Liu, R.-S. *J. Am. Chem. Soc.* **1979**, *101*, 491.
(33) Murugesu, M.; Abboud, K. A.; Christou, G. *Polyhedron* **2004**, *23*, 2779.
(34) Tanase, T.; Inagaki, T.; Yamada, Y.; Kato, M.; Ota, E.; Yamazaki, M.; Sato, M.; Mori, W.; Yamaguchi, K.; Mikuriya, M.; Takahashi, M.; Takeda, M.; Kinoshita, I.; Yano, S. **1998**, *4*, 713.
(35) Stibrany, R. T.; Gorun, S. M. *Angew. Chem., Int. Ed. Engl.* **1990**, *29*, 1156.
(36) McCusker, J. K.; Christmas, C. A.; Hagen, P. M.; Chadha, R. K.; Jarvey, D. F.; Hendrickson, D. N. *J. Am. Chem. Soc.* **1991**, *113*, 6114.
(37) Christmas, C. A.; Tsai, H.-L.; Pardi, L.; Kesselman, J. M.; Gantzel, P. K.; Chadha, R. K.; Gatteschi, D.; Jarvey, D. F.; Hendrickson, D. N. *J. Am. Chem. Soc.* **1993**, *115*, 12483.
(38) Micklitz, W.; Lippard, S. J. *J. Inorg. Chem.* **1988**, *27*, 3067.
(39) Micklitz, W.; Bott, S. G.; Bentsen, J. G.; Lippard, S. J. *J. Am. Chem. Soc.* **1989**, *111*, 372.

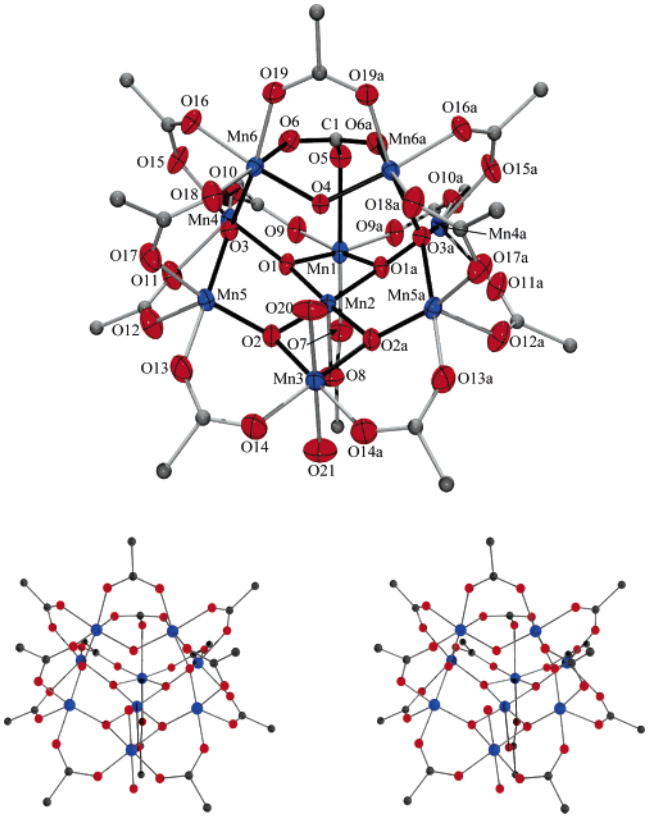

Figure 6. ORTEP representation in PovRay format of complex **6** at the 30% probability level, together with a stereopair. For clarity, the hydrogen atoms have been omitted, and only the quaternary C atoms of the ligands are shown: Mn^{III}, blue; O, red; C, gray.

Table 4. Selected Distances (Å) and Angles[a] (deg) for Complex **6**

Mn(1)−O(1)	1.885(3)	Mn(4)−O(15)	1.943(4)
Mn(1)−O(9)	1.933(4)	Mn(4)−O(11)	2.081(5)
Mn(1)−O(7)	2.111(7)	Mn(4)···Mn(6)	3.1767(10)
Mn(1)−O(5)	2.425(7)	Mn(5)−O(3)	1.865(3)
Mn(1)···Mn(2)	2.8126(14)	Mn(5)−O(2)	1.882(4)
Mn(2)−O(1)	1.900(3)	Mn(5)−O(13)	1.923(4)
Mn(2)−O(2)	1.906(4)	Mn(5)−O(17)	1.975(4)
Mn(2)−O(8)	2.192(6)	Mn(5)−O(12)	2.041(5)
Mn(2)···Mn(3)	2.8313(15)	Mn(6)−O(4)	1.849(2)
Mn(3)−O(2)	1.868(4)	Mn(6)−O(3)	1.885(3)
Mn(3)−O(14)	1.936(5)	Mn(6)−O(19)	1.928(4)
Mn(3)−O(20)	2.245(6)	Mn(6)−O(16)	1.969(4)
Mn(3)−O(21)	2.261(10)	Mn(6)−O(18)	2.155(4)
Mn(4)−O(1)	1.861(3)	Mn(6)−O(6)	2.321(4)
Mn(4)−O(3)	1.882(3)	O(5)−C(1)	1.274(8)
Mn(4)−O(10)	1.934(4)	O(6)−C(1)	1.303(5)
C(1)−O(5)−Mn(1)	118.6(5)	O(5)−C(1)−O(6)	118.0(3)
C(1)−O(6)−Mn(6)	133.5(3)	O(6)−C(1)−O(6a)	118.3(5)

[a] Full listings in the Supporting Information.

mirror plane of the molecule. Bond valence sum (BVS) calculations[27] indicate that all the Mn ions are in the +3 oxidation state. Atom Mn(2) is five-coordinate with exactly square-pyramidal (sp) geometry ($\tau = 0$, where $\tau = 0$ and 1 for ideal sp and trigonal-bipyramidal geometries, respectively[40]) as a result of the crystallographically imposed mirror plane symmetry. Atoms Mn(4) and Mn(5) are also five-coordinate with sp and distorted sp geometries ($\tau = 0.01$ and 0.22, respectively). The remaining Mn^{III} centers all possess distorted octahedral geometries.

Each octahedral Mn^{III} displays a clear JT axial elongation, with axial Mn−O bonds approximately 0.20 Å longer than equatorial ones. For Mn(2), the axial Mn(2)−O(8) length [2.192(6) Å] is longer than basal lengths [1.900(3)−1.906(4) Å], as expected for sp geometry. This is similarly the case for sp Mn(4) and Mn(5) [Mn(4)−O(11) = 2.081(5) and Mn(5)−O(12) = 2.041(5) Å]. In effect, there is parallel alignment of the JT distortion axes of the three Mn^{III} ions of the $[Mn_3O_4]$ base [Mn(1), Mn(2), Mn(3)], whereas there is an overall random alignment of the distortion axes of the remaining Mn centers. This will be of relevance to the magnetic discussion later (vide infra).

The Mn_9 core of **6** is very similar to that in $[Mn_9O_7(O_2CPh)_{13}(py)_2]$,[41] $[Na_2Mn_9O_7(O_2CPh)_{15}(MeCN)_2]$,[42] and $[K_2Mn_9O_7(O_2CBu^t)_{15}(HO_2CBu^t)_2]$.[43] The core also appears as a subunit in the larger cluster $[Mn_{22}O_{12}(O_3PPh)_8(O_2CEt)_{22}(H_2O)_8]$.[44] The primary difference between complex **6** and these other Mn_9 clusters is the triply bridging CO_3^{2-} ligand that fuses the handle to the $[Mn_7O_4]$ basket subunit. Triply bridging carbonate ions are somewhat rare in discrete transition metal clusters, especially in Mn chemistry. Known clusters with such $\eta^1,\eta^1,\eta^1,\mu_3$-$CO_3^{2-}$ ligands include a handful of molecules containing Cu,[45] Z,[45d,e,46] V,[47] and Mo.[48] To our knowledge, complex **6** is the first example of a triply bridging CO_3^{2-} ion in molecular Mn chemistry. There is, however, a doubly bridging, η^1,η^1,μ-CO_3^{2-} ligand in Mn(II) chemistry, although it was not crystallographically confirmed.[23] A heterometallic Mn_{16} cluster in which a carbonate group bridges equatorial Ba^{2+} ions has also been reported.[49] The carbonate ligand in **6** is not planar; the carbon atom C(1) is slightly (0.18 Å) out of the plane formed by the three oxygen atoms [O(5), O(6), and O(6a)]. All previous $\eta^1,\eta^1,\eta^1,\mu_3$-$CO_3^{2-}$ groups are planar, and we assign the

(40) Jansen, J. C.; Van Koningsveld, H.; Van Ooijen, J. A. C.; Reedijk, J. *Inorg. Chem.* **1980**, *19*, 170.

(41) Low, D. W.; Eichhorn, D. M.; Draganescu, A.; Armstrong, W. H. *Inorg. Chem.* **1991**, *30*, 877.

(42) Tsai, H.-L.; Wang, S.; Folting, K.; Streib, W. E.; Hendrickson, D. N.; Christou, G. *J. Am. Chem. Soc.* **1995**, *117*, 2503.

(43) Murrie, M.; Parsons, S.; Winpenny, R. E. P. *Dalton Trans.* **1998**, *9*, 1423.

(44) Brockman, J. T.; Wernsdorfer, W.; Abboud, K. A.; Christou, G. Unpublished results.

(45) (a) Kolks, G.; Lippard, S. J.; Waszczak, J. V. *J. Am. Chem. Soc.* **1980**, *102*, 4833. (b) van Albada, G. A.; Mutikainen, I.; Roubeau, O.; Turpeinen, U.; Reedijk, J. *Inorg. Chim. Acta* **2002**, *331*, 208. (c) Escuer, A.; Vicente, R.; Peñalba, E.; Solans, X.; Font-Bardía, M. *Inorg. Chem.* **1996**, *35*, 248. (d) Bazzicalupi, C.; Bencini, A.; Bianchi, A.; Corana, F.; Fusi, V.; Giorgi, C.; Paoli, P.; Paoletti, P.; Valtancoli, B.; Zanchini, C. *Inorg. Chem.* **1996**, *35*, 5540. (e) Mao, Z.-W.; Liehr, G.; van Eldik, R. *Dalton Trans.* **2001**, *10*, 1593. (f) Rodríguez, M.; Llobet, A.; Corbella, M.; Müller, P.; Usón, M. A.; Martell, A. E.; Reibenspies, J. *Dalton Trans.* **2002**, *14*, 2900. (g) van Albada, G.; Mutikainen, I.; Roubeau, O. S.; Turpeinen, U.; Reedijk, J. *Eur. J. Inorg. Chem.* **2000**, *10*, 2179.

(46) (a) Mann, K. L. V.; Jeffery, J. C.; McCleverty, J. A.; Ward, M. D. *Dalton Trans.* **1998**, *18*, 3029. (b) Schrodt, A.; Neubrand, A.; van Eldik, R. *Inorg. Chem.* **1997**, *36*, 4579. (c) Trösch, A.; Vahrenkamp, H. *Inorg. Chem.* **2001**, *40*, 2305. (d) Bazzicalupi, C.; Bencini, A.; Bianchi, A.; Fusi, V.; Paoletti, P.; Valtancoli, B. *Chem. Commun.* **1995**, *15*, 1555. (e) Chen, X.-M.; Deng, Q.-Y.; Wang, G.; Xu, Y.-J. *Polyhedron* **1994**, *13*, 3085. (f) Murthy, N. N.; Karlin, K. D. *Chem. Commun.* **1993**, *15*, 1236.

(47) Yamase, T.; Ohtaka, K. *Dalton Trans.* **1994**, *18*, 2599.

(48) Cotton, F. A.; Lin, C.; Murillo, C. A. *J. Am. Chem. Soc.* **2001**, *123*, 2670.

(49) (a) Lee, J.; Chasteen, N. D.; Zhao, G.; Papaefthymiou, G. C.; Gorun, S. M. *J. Am. Chem. Soc.* **2002**, *124*, 3024. (b) Lee, J.; Gorun, S. M. *Angew. Chem., Int. Ed.* **2003**, *42*, 1512.

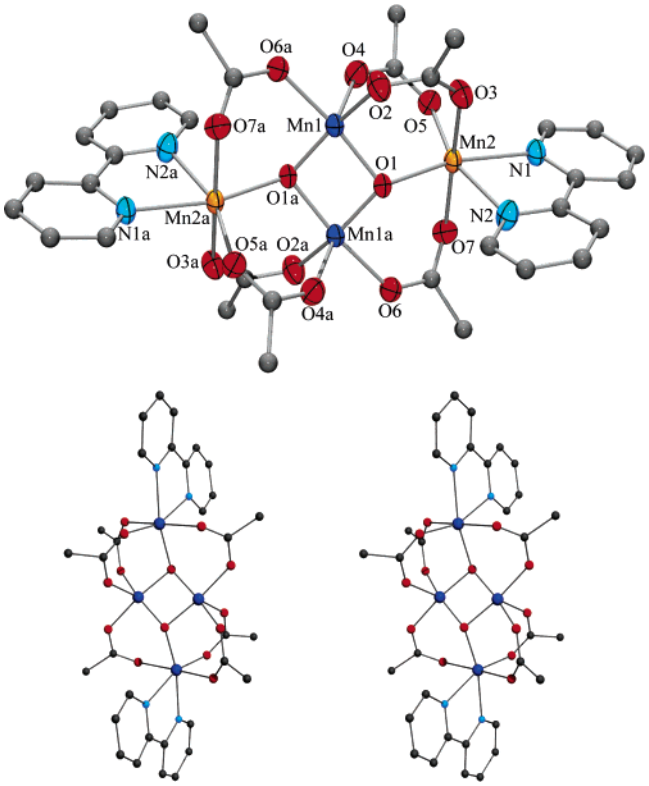

Figure 7. ORTEP representation in PovRay format of complex **7** at the 50% probability level, together with a stereopair. For clarity, the hydrogen atoms have been omitted, and only the quaternary C atoms of the ligands are shown: Mn^{III}, blue; Mn^{II}, orange; O, red; C, gray; N, cyan.

Table 5. Selected Distances[a] (Å) for Complex **7**

Mn(1)−O(1a)	1.8537(18)	Mn(2)−O(1)	2.0906(18)
Mn(1)−O(1)	1.8560(18)	Mn(2)−O(5)	2.1201(19)
Mn(1)−O(2)	1.957(2)	Mn(2)−O(3)	2.184(2)
Mn(1)−O(6a)	1.965(2)	Mn(2)−O(7)	2.212(2)
Mn(1)−O(4)	2.089(2)	Mn(2)−N(1)	2.259(2)
Mn(1)−Mn(1a)	2.7755(8)	Mn(2)−N(2)	2.281(2)

[a] Full listings in the Supporting Information.

slightly pyramidal structure in **6** to the strain the CO_3^{2-} group experiences in the bridging mode it adopts. The bond distances C(1)−O(5) (1.274(8) Å) and C(1)−O(6) and C(1)−O(6a) (1.303(5) Å) are in agreement with a CO_3^{2-} ion. The C−O bond lengths in formaldehyde, free carbonate anion, and methanol are 1.22, 1.33, and 1.43 Å, respectively.

A labeled ORTEP[25] plot in PovRay format of complex **7** is shown in Figure 7. Selected interatomic distances are listed in Table 5. Complex **7**·$2H_2O$ crystallizes in the monoclinic space group $P2_1/c$. The asymmetric unit contains half the molecule and two H_2O solvent molecules. The structure consists of a $[Mn^{III}_2Mn^{II}_2(\mu_3\text{-}O)_2]^{6+}$ core with peripheral ligation provided by six bridging $Pe^tCO_2^-$ ligands and two terminal bipyridine molecules. BVS calculations[27] indicate that Mn(1) and Mn(1a) are in the +3 oxidation state while Mn(2) and Mn(2a) are in the +2 oxidation level. Each Mn^{II} center is in a distorted octahedral environment, while the two Mn^{III} centers are five-coordinate with distorted sp geometry ($\tau = 0.16$).[40]

The complex possesses an exactly planar array of four Mn atoms bridged by two μ_3-oxide atoms, O(1) and O(1a), one above and one below the Mn_4 plane. The distance of the

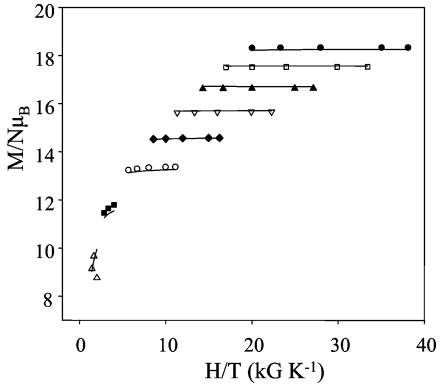

Figure 8. Plot of reduced magnetization ($M/N\mu_B$) vs H/T for a dried microcrystalline sample of complex **4**·$2CH_2Cl_2$ at 5 (●), 10 (□), 20 (▲), 30 (▽), 40 (◆), 50 (○), 60 (■), and 70 (△) kG in eicosane. The solid lines are the fit of the data; see the text for the fit parameters.

μ_3-oxygen atoms above or below the Mn_4 plane is 0.60 Å. The $[Mn^{III}_2Mn^{II}_2(\mu_3\text{-}O)_2]^{6+}$ core can be considered as two edge-sharing $[Mn_3O]$ units. Each edge of the Mn_4 rhombus is bridged by either one or two μ-$^tPeCO_2^-$ groups. The edges bridged by only one *tert*-pentylate ligand have a slightly longer Mn···Mn separation [3.465 Å] than those bridged by two *tert*-pentylate groups [3.274 Å]. The central Mn(1)···Mn(1a) separation is significantly shorter [2.775 Å], consistent with the two oxide bridges. Two terminal bpy groups complete the peripheral ligation, one at each end of the molecule. The local z axes of the two five-coordinate Mn^{III} centers, Mn(1)−O(4) = 2.089(2) and Mn(1a)-O(4a) = 2.089(2), are oriented parallel to each other. The overall symmetry of the complex is C_i. The overall structure of complex **7** is nearly identical to that observed in $[Mn_4O_2(O_2CMe)_6(bpy)_2]$.[50]

Magnetic Susceptibility Studies of Complex 4. Variable-temperature DC susceptibility measurements were performed in the 5.0−300 K range on a powdered microcrystalline sample of **4**·$2CH_2Cl_2$, restrained in eicosane to prevent torquing, in a 5 kG field. The value of $\chi_M T$ in the 150−300 K range, 20−22 cm^3 K mol^{-1}, rapidly increases to a maximum of 53 cm^3 K mol^{-1} at 15 K before decreasing rapidly at lower temperatures. The maximum value indicates a large ground-state spin (S) value, and the decrease of $\chi_M T$ at low temperatures is primarily due to Zeeman and zero-field splitting (ZFS) effects.

A theoretical treatment of the susceptibility data using the Kambé vector coupling approach was not feasible due to the topological complexity and low symmetry of the Mn_{12} cluster. Instead, our efforts were focused on the determination of the ground-state spin by variable-temperature and -field magnetization (M) measurements in the 1.8−4.00 K temperature and 0.5−7 T field ranges. The data are plotted as reduced magnetization ($M/N\mu_B$) versus H/T in Figure 8, where N is Avogadro's number, μ_B is the Bohr magneton, and H is the applied magnetic field. For complexes populating only the ground state and experiencing no ZFS, the

(50) Vincent, J. B.; Christmas, C.; Chang, H.-R.; Li, Q.; Boyd, P. D. W.; Huffman, J. C.; Hendrickson, D. N.; Christou, G. *J. Am. Chem. Soc.* **1989**, *111*, 2086.

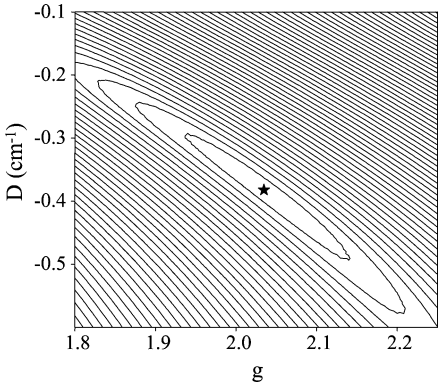

Figure 9. Two-dimensional contour plot of the error surface for the D vs g fit for complex **4**·$2CH_2Cl_2$.

magnetization follows the Brillouin function and the isofield lines all superimpose and saturate at a value of gS. The data in Figure 8 show that the isofield lines do not superimpose for complex **4**, indicating that the ground state is zero-field split. The data were fit using the method described elsewhere[50,51] that involves diagonalization of the spin Hamiltonian matrix, assuming only the ground state is occupied at these temperatures, and including axial ZFS Zeeman interactions and a full powder average of the magnetization. Fitting of the data gave $S = 10$, $g = 2.03$, and $D = -0.38$ cm^{-1}. These values are typical of neutral Mn_{12} complexes; complex **4** has the same spin as its parent complex **1**. Thus, replacement of the water ligands with methanol groups does not significantly perturb the properties of the Mn_{12} complex.

To confirm that the obtained parameters were the true global rather than local minimum, and to assess the uncertainty in the obtained g and D values, a root mean square D vs g error surface for the fit was generated using the program GRID.[52] The error surface is shown in Figure 9 as a contour plot for the $D = -0.10$ to -0.60 cm^{-1} and $g = 1.8$ to 2.25 ranges. One soft fitting minimum is observed; the contour describes the region of minimum error from $D \approx -0.30$ to -0.49 cm^{-1} and $g \approx 1.94$ to 2.14, giving fitting parameters of $D = -0.39 \pm 0.10$ cm^{-1} and $g = 2.0 \pm 0.1$.

To confirm, as expected, that this new Mn_{12} complex is a SMM, and to assess further the influence of its terminal MeOH groups instead of the usual H_2O ones, AC magnetic susceptibility studies were carried out on dried, microcrystalline samples of **4**·$2CH_2Cl_2$ in the 1.8−10 K range in a 3.5 G AC field with oscillation frequencies (υ) up to 1500 Hz. All other previously characterized Mn_{12} complexes exhibit at least one frequency-dependent out-of-phase (χ_M'') signal that is accompanied by a frequency-dependent decrease in the in-phase (χ_M') signal, indicating slow magnetization relaxation. Although such signals are not sufficient proof of the SMM property, they are a strong indicator that a complex behaves as a SMM. Indeed, χ_M'' AC susceptibility signals are clearly exhibited by complex **4**·$2CH_2Cl_2$ (Figure 10). In fact, there are two such signals, corresponding to two

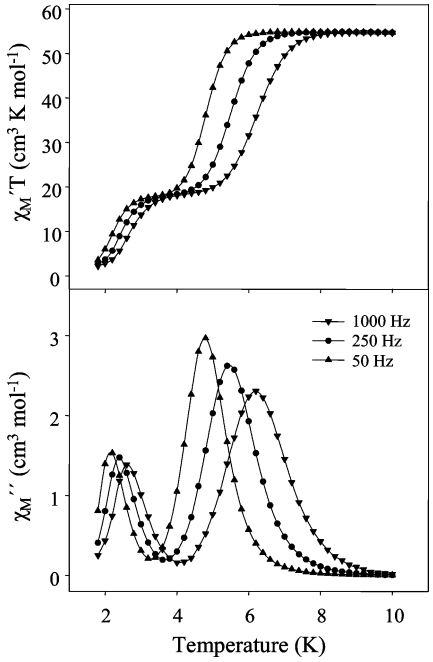

Figure 10. Plot of the in-phase (as $\chi_M'T$) and out-of-phase (χ_M'') AC susceptibility signals vs temperature for complex **4**·$2CH_2Cl_2$ at the indicated oscillation frequencies.

distinct relaxation processes, a higher temperature (HT) peak at ~6 K and a lower temperature (LT) peak at ~2.5 K. The signals are accompanied by two frequency-dependent decreases in the in-phase $\chi_M'T$ plot, first at $T \sim 7.5$ K and then at $T \sim 3$ K, respectively, indicating that the magnetization of **4** cannot relax fast enough to stay in-phase with the oscillating field and that complex **4** is most likely a SMM.

The presence of two peaks in the out-of-phase AC susceptibility plot of **4** is typical of Mn_{12} complexes and has been shown previously to be due to JT isomerism, in which complexes differ in the relative orientation of one or more Mn^{III} JT elongation axes.[15,31,53,54] The LT (faster relaxing) isomer is the one with the abnormal orientation of the JT axis toward the bridging oxide ions, whereas the HT (slower relaxing) form is that with all JT axes avoiding bridging oxide ions. Normally, the HT form is the predominant form in wet crystals, with the LT form often becoming more pronounced in dried solids as interstitial solvent of crystallization is lost. Indeed, the HT:LT ratio in dried solid of **4** is 3:1 (Figure 10), whereas it is 19:1 in wet crystals. The significantly smaller amount of the LT form in the latter also rationalizes why it is not observed in the X-ray crystal structure of the complex, since the small fraction of the LT form and the likely static disorder of the abnormally oriented axis over multiple sites will dilute its effect on the structural parameters.

The value of $\chi_M'T$ in the temperature-independent region of Figure 10 is especially useful for estimating the ground-state spin without interference from even a small DC field.

(51) Hendrickson, D. N.; Christou, G.; Schmitt, E. A.; Libby, E.; Bashkin, J. S.; Wang, S.; Tsai, H.-L.; Vincent, J. B.; Boyd, P. D. W.; Huffman, J. C.; Folting, K.; Li, W.; Streib, W. E. *J. Am. Chem. Soc.* **1992**, *114*, 2455.
(52) Davidson, E. R. *GRID*; Indiana University: Bloomington, IN, 1999.
(53) Sun, Z.; Ruiz, D.; Dilley, N. R.; Soler, M.; Ribas, J.; Folting, K.; Maple, M. B.; Christou, G.; Hendrickson, D. N. *Chem. Commun.* **1999**, *19*, 1973.
(54) Zhao, H.; Berlinguette, C. P.; Basca, J.; Prosvirin, A. V.; Bera, J. K.; Tichy, S. E.; Schelter, E. J.; Dunbar, K. R. *Inorg. Chem.* **2004**, *43*, 1359.

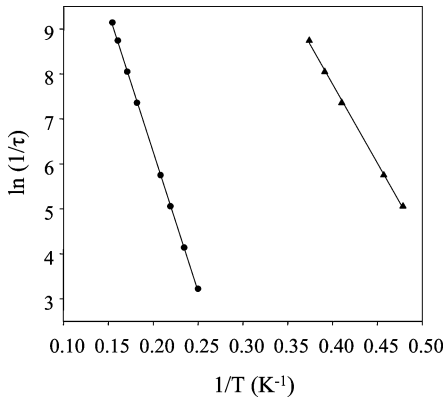

Figure 11. Plot of the natural logarithm of the relaxation rate, $\ln(1/\tau)$, vs $1/T$ for a dried, microcrystalline sample of complex **4**·$2CH_2Cl_2$ using AC χ_M'' data: (●) the HT peak (slower relaxing species) and (▲) the LT peak (faster relaxing species). The solid lines are fits to the Arrhenius equation; see the text for the fit parameters.

The $\chi_M'T$ value above 7 K of ~54 cm^3 K mol^{-1} for **4** corresponds to an $S = 10$ system with $g = 1.98$, consistent with the DC magnetization results above.

At the χ_M'' peak maximum, the magnetization relaxation rate ($1/\tau$, where τ is the relaxation time) is equal to the angular frequency ($2\pi\upsilon$) of the AC field, and thus χ_M'' vs υ studies provide rate vs T kinetic data,[55] and these were fit to the Arrhenius equation:

$$1/\tau = 1/\tau_0 \exp(-U_{eff}/kT) \quad (3)$$

This is the characteristic behavior of a thermally activated Orbach process, where U_{eff} is the effective energy barrier, k is the Boltzmann constant, and $1/\tau_0$ is the preexponential term. The frequency dependencies of the χ_M'' peaks for **4** were determined at different oscillation frequencies in the 5−1500 Hz range. A plot of $\ln(1/\tau)$ vs $1/T$ using this χ_M'' vs T data is shown in Figure 11, with the least-squares fit to eq 3 shown as solid lines for both the HT (●) and LT (▲) signals. The effective energy barrier to magnetization relaxation (U_{eff}) for the HT signal (slower relaxing species) is 43 cm^{-1} (62 K), while that of the LT signal (faster relaxing species) is much smaller, 24 cm^{-1} (35 K). These are very similar to the values previously found for such HT and LT signals within the $[Mn_{12}O_{12}(O_2CR)_{16}(H_2O)_4]$ family.[15,53] The values of the preexponential factor, $1/\tau_0$, 1.29×10^8 s^{-1} for the HT peak and 2.98×10^{10} s^{-1} for the LT peak, are also within the range normally found for the $[Mn_{12}O_{12}(O_2CR)_{16}(H_2O)_4]$ family.

Finally, we should add that we have not complemented the above results on **4** with single-crystal hysteresis studies using a micro-SQUID apparatus to investigate the effect, if any, of the bulky carboxylate groups on the hysteresis loops. While we are very interested in this general point, such studies are instead currently in progress in great detail with the $Bu^tCH_2CO_2^-$ derivatives, and these results will be reported separately.

Magnetic Susceptibility Studies of Complexes 5−8. Variable-temperature DC susceptibility measurements were performed on dried, microcrystalline samples of **5**·$^1/_2CH_2Cl_2$·$4H_2O$, **6**·HO_2CPe^t, **7**·$2H_2O$, and **8**·$^1/_2MeNO_2$, restrained in eicosane to prevent torquing, in a 1 kG field in the range of 5.0−300 K (see Supporting Information). For **5**, χ_MT smoothly decreases from 15.8 cm^3 K mol^{-1} at 300 K to 3.9 cm^3 K mol^{-1} at 5.0 K. The value at 300 K is less than the 18 cm^3 K mol^{-1} spin-only value ($g = 2.0$) expected for a Mn^{III}_6 complex with noninteracting metal centers, indicating the presence of appreciable antiferromagnetic interactions between the manganese centers. For **6**, the χ_MT value of 4.0 cm^3 K mol^{-1} at 300 K decreases gradually with decreasing temperature to 0.35 cm^3 K mol^{-1} at 5.0 K, while the χ_MT value for **8** of 19.3 cm^3 K mol^{-1}at 300 K decreases gradually to 2.4 cm^3 K mol^{-1} at 5.0 K. The spin-only ($g = 2$) value for a molecule composed of noninteracting Mn^{III}_9 ions is 27 cm^3 K mol^{-1}. The χ_MT value of 7.4 cm^3 K mol^{-1} at 300 K for complex **7** gradually decreases with decreasing temperature to 3.5 cm^3 K mol^{-1} at 5.0 K. The value of χ_MT at 300 K is less than the spin-only value for a unit composed of noninteracting $Mn^{II}_2Mn^{III}_2$ ions (14.75 cm^3 K mol^{-1}). Hence, the molecules all appear to have appreciable intramolecular antiferromagnetic interactions and relatively low or zero ground-state spin values.

Complex **5** contains six Mn^{III} centers with total spin values ranging from 0 to 12, while complexes **6** and **8** each contain nine Mn^{III} centers with total spin values ranging from 0 to 18. Again, it is not possible to easily evaluate the various exchange parameters between the Mn centers as a result of the complexity and low symmetry of the clusters. In addition, magnetization data collected in the 0.1−70 kG and 1.8−10.0 K field and temperature ranges could not be satisfactorily fit to a model that assumes only the ground state is populated. This behavior is typical of (i) complexes with low ground-state S values, which cross with excited states with larger S values as a result of Zeeman effects in the applied DC field, and/or (ii) low-lying excited states from weak exchange interactions and/or spin frustration effects[56] within the complicated topologies present in most of these complexes. The exception to the latter is tetranuclear complex **7**, but even this has Mn^{II}/Mn^{III} interactions, which are typically very weak, and spin frustration within the triangular Mn_3 subunits. In any event, further analysis of the exchange interactions within **7** was not pursued since the DC magnetic susceptibility behavior of such butterfly clusters has been already thoroughly studied.[50]

Overall, the low-temperature DC magnetic susceptibility studies and the profiles of the susceptibility vs T plots (Supporting Information) suggest small ground-state spin values of $S \leq 2$ for complexes **5**·$^1/_2CH_2Cl_2$·$4H_2O$, **6**·HO_2CPe^t, **7**·$2H_2O$, and **8**·$^1/_2MeNO_2$. Further assessment of the values was carried out using AC susceptibility studies in a 3.5 G AC field oscillating at frequencies up to 997 Hz. While

(55) Novak, M. A.; Sessoli, R. In *Quantum Tunneling of Magnetization—QTM '94*; Gunther, L., Barbara, B., Eds.; Kluwer: Amsterdam, 1995; pp 171−188.

(56) (a) Castro, S. L.; Sun, Z.; Grant, C. M.; Bollinger, J. C.; Hendrickson, D. N.; Christou, G. *J. Am. Chem. Soc.* **1998**, *120*, 2365. (b) Albela, B.; El Fallah, M. S.; Ribas, J.; Folting, K.; Christou, G.; Hendrickson, D. N. *Inorg. Chem.* **2001**, *40*, 1037.

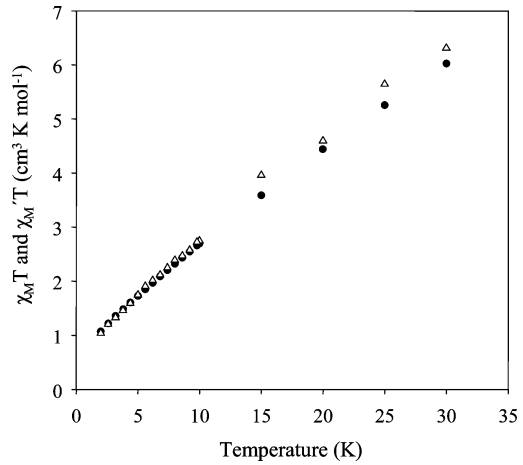

Figure 12. Plot of $\chi_M'T$ vs temperature for complex **6**·HO_2CPe^t in the 2.0−30.0 K range from AC magnetic susceptibility measurements (△), including the DC $\chi_M T$ data (●) for this temperature range. The AC data were measured with a 3.5 G AC field oscillating at 997 Hz.

the appearance of an out-of-phase AC susceptibility signal (χ_M'') is indicative of the onset of slow magnetic relaxation, the in-phase signal (χ_M') can indicate, as mentioned earlier, the ground-state *S* value and whether low-lying excited states are populated even at very low temperatures. Specifically, a temperature-independent $\chi_M'T$ vs *T* plot indicates that only the ground-state spin state is populated, while a sloping $\chi_M'T$ vs *T* plot indicates population of low-lying excited states. As expected on the basis of the DC studies, the $\chi_M'T$ vs *T* plots of each of the complexes are strongly sloping with decreasing values of $\chi_M'T$ with decreasing temperature, indicating depopulation of excited states with greater *S* values than the ground state. Comparison of $\chi_M'T$ with $\chi_M T$ over the same *T* range shows that the two are essentially superimposable for each of the clusters, as shown in Figure 12 for representative complex **6**·HO_2CPe^t. Linear extrapolation suggests that the plot for **6** is heading for $\chi_M T \leq 0.6$ cm^3 K mol^{-1} at 0 K, a value consistent with at most an $S = 1$ ground-state spin, and more likely $S = 0$. Similarly, the AC data for **5, 7**, and **8** suggest $S \leq 2$ (and probably 1 or 0), but with very low-lying excited states that are populated even at 1.8 K and which make a more precise assignment of a ground-state value very difficult.

Conclusions

The use of the basic, hydrophobic carboxylic acid, *tert*-pentylic acid, as a reactant in Mn_{12} chemistry has led to the isolation of several new Mn clusters, two of which are new structural types in Mn chemistry. The reaction of $[Mn_{12}O_{12}(O_2CPe^t)_{16}(H_2O)_4]$ (**3**) with MeOH in the presence of *tert*-pentylic acid have led to the isolation of $[Mn_{12}O_{12}(O_2CPe^t)_{16}(MeOH)_4]$ (**4**), a new member of a subclass of Mn_{12} clusters in which the water ligands that coordinate to either three or four Mn^{III} ions in the outer ring of the cluster have been replaced by another ligand, MeOH. Magnetic studies on **4** suggest that the complex retains an $S = 10$ ground-state spin as expected for a neutral Mn_{12} cluster. Additionally, peaks in the out-of-phase AC susceptibility indicate the onset of slow magnetization relaxation and suggest that **4** functions as a SMM.

In contrast, recrystallization of **3** from $CH_2Cl_2/MeNO_2$ in the presence of *tert*-pentylic acid causes a structural change and affords two new structural types in Mn chemistry, $[Mn_6O_2(O_2CH_2)(O_2CPe^t)_{11}(HO_2CPe^t)_2(O_2CMe)]$ (**5**) and $[Mn_9O_6(OH)(CO_3)(O_2CPe^t)_{12}(H_2O)_2]$ (**6**). Complex **5** contains only the third example of a μ_4-methanediolate unit, while complex **6** possesses a nonplanar, triply bridging CO_3^{2-} anion and is the first example of a discrete complex with three Mn ions bridged by a carbonate group. These investigations emphasize the differences in the reactivity of the nearly identical Mn_{12} complexes, **2** and **3**; recrystallization of **2** under similar conditions results in the retention of the $[Mn_{12}O_{12}]^{16+}$ core. In addition, the reaction of **3** with the chelating ligand, 2,2′-bipyridine, has afforded $[Mn_4O_2(O_2CPe^t)_6(bpy)_2]$ (**7**). Structural rearrangement of the $[Mn_{12}O_{12}]^{16+}$ core is also observed when **2** undergoes reactions with other chelating ligands. Further investigations to probe the reactivity of **2** with various solvents, including THF, has led to the isolation of a new enneanuclear cluster, $[Mn_9O_7(O_2CCH_2Bu^t)_{13}(THF)_2]$ (**8**). Magnetic studies on complexes **5**−**8** suggest ground-state spin values of $S \leq 2$ and show that the complexes do not function as single-molecule magnets.

Electrochemical studies on both complexes **2** and **4** reveal that, in contrast to most other characterized Mn_{12} clusters, these molecules exhibit irreversible reduction processes, supporting the proposal that reductive destabilization of the $[Mn_{12}O_{12}]$ core followed by structural rearrangement occurs to yield new clusters of differing nuclearity and topology. While the strongly electron-donating nature of the ligands coordinated to the metal centers in **2** and **4** accounts for the unwillingness of the cluster to accept another electron reversibly, it also accounts for the quasireversible oxidation wave, a process that occurs at a potential nearly 1 V lower than previously found for other Mn_{12} clusters.

Acknowledgment. This work was supported by the National Science Foundation.

Supporting Information Available: Plots of $\chi_M'T$ from AC magnetic susceptibility measurements and/or $\chi_M T$ from DC magnetic susceptibility measurements in a 10 kG field vs *T* for complexes **5**·$^1/_2CH_2Cl_2$·$4H_2O$, **6**·HO_2CPe^t, **7**·$2H_2O$, and **8**·$^1/_2MeNO_2$ and X-ray crystallographic files in CIF format and complete listing of bond distances and angles for complexes **4**·2MeCN, **5**·$^1/_2CH_2Cl_2$, **6**·H_2O·HO_2CPe^t, and **7**·$2H_2O$. This material is available free of charge via the Internet at http://pubs.acs.org.

IC050201+